2023

Expansion on the Use of the Novel Compound, ELP-004, Using a Mycobacterium tuberculosis Experimentation Model

Kendyl Marie Berry
West Virginia University, kendylberry415@gmail.com

Expansion On the Use of the Novel Compound, ELP-004, Using a *Mycobacterium tuberculosis* Experimentation Model

Kendyl Berry

Thesis submitted to the School of Medicine at West Virginia University

in partial fulfillment of the requirements for the degree of

Master of Science in Biomedical Sciences

Werner J. Geldenhuys, Ph.D., M.S., Chair

John B. Barnett, Ph.D.

Ivan Martinez, Ph.D.

Department of Microbiology, Immunology, and Cell Biology

Morgantown, WV

2023

Keywords: *Mycobacterium tuberculosis,* tuberculosis, osteoarticular tuberculosis, bone erosion, RAW264.7 cells

Abstract

Expansion Upon the Use of the Novel Compound, ELP-004, Using a *Mycobacterium tuberculosis* Experimentation Model

Kendyl Berry

Osteoarticular tuberculosis (OAT) is a bone degenerative disease that results in bone erosion, joint effusion, joint swelling, and sometimes, nerve compression. OAT occurs from the hematogenous dissemination of *Mycobacterium tuberculosis (Mtb)* bacilli spreading from the primary site of infection to the bones and joints; the primary site of infection tends to be the lungs as pulmonary tuberculosis infections are the most common. OAT can occur as the result of an active or latent infection. Latent infections result in OAT when bacilli are able to escape granulomas. The incidence of OAT is not as high as pulmonary infections, making up about 10-15% of all extrapulmonary tuberculosis infections. Currently, the only treatment available for OAT is the standard regimen of care for treating tuberculosis; this includes 4-6 months of antibiotic treatment. Antibiotic treatment can be extended up to 12+ months for extrapulmonary TB. This does not resolve bone degeneracies or deformities that occur as a result of OAT. The novel compound, ELP-004, reduces bone erosion in mouse models of arthritis. To determine the effectiveness of ELP-004 in the treatment of OAT, a tuberculosis experimentation model was set up in vitro and in vivo. The in vivo model used RAW264.7 cells, a mouse monocyte/macrophage cell line commonly used to study osteoclastogenesis. RAW264.7 cells were exposed to extract from the H37Rv strain of *Mtb* did not result in TRAP positive syncytial formation; however, exposure to this TB extract still resulted in multinucleation. Cells exposed to *Mtb* extract also could not mobilize calcium matrices, and qPCR analysis revealed that osteoclast formation markers were absent. Although osteoclast-like cells could not be formed with this model, treatment with ELP-004 resulted in a knockdown of syncytial cells, showing promise for its use in patients. Work on the in vitro model ceased to continue and a reevaluation of the model is necessary. Since ELP-004 was able to knockdown multinucleation in vitro, it was important to determine if the drug could be used in combination with current tuberculosis treatments. Using two first-line antibiotics, rifampin and isoniazid, the metabolism of combination therapy was assessed using cytochrome P450 enzymes (CYP). Cytochrome P450 enzymes are responsible for the metabolism of 90% of all drugs and xenobiotics. They are located primarily in the liver and are responsible for phase I metabolism. Of the CYPs tested, only *Cyp1a2* and *Cyp2b10* had increased mRNA expression. Using a western blot to confirm protein expression, only CYP2B10 showed increased protein expression. With this data, it can be concluded that CYP2B6, the human equivalent of CYP2B10, is the primary induced metabolic pathway for the combination therapy. These data combined show promise for using ELP-004 to treat bone erosion from a tuberculosis infection. The ability of ELP-004 to inhibit increased osteoclastogenesis in an arthritis model can be expanded to prevent enhanced osteoclastogenesis in OAT.

Table of Contents

List of Figures

List of Tables

Chapter 1

Introduction

Tuberculosis

Tuberculosis (TB) is a global public health crisis, and while primarily affecting low and middle-income countries, TB affects people of all countries and all age groups. Even with incidence of infection decreasing by 11% between 2015 and 2020, in 2021 alone, there were an estimated 10.6 million cases, with 1.5 million deaths, making TB the second leading infectious killer after SARS-CoV-2 worldwide (World Health Organization - WHO). The pathogenesis, expensive, long and regimented treatment, ineffective vaccine, and the unavailability of proper diagnostic tools, particularly in endemic areas, continues the spread of tuberculosis. Furthermore, the increasing prevalence of drug-resistant TB hinders infection control (Delogu et al., 2013, Seung et al., 2015).

The bacterium *Mycobacterium tuberculosis* (*Mtb*) is the etiological agent of tuberculosis. *Mtb* is a large, aerobic, non-spore forming, non-motile bacillus whose primary route of infection is through airborne droplets such as coughing and sneezing (Natarajan et al., 2020). Upon infection, *Mtb* binds to complement receptors located on alveolar macrophages and is phagocytized as a part of the innate response (Natarajan et al., 2020). Following phagocytosis, *Mtb* reduces the acidity of the phagosome and lipoarabinomannan, disrupting the formation of the phagolysosome (Natarajan et al., 2020). When phagolysosome formation is successfully arrested, the mycobacteria replicate and burst from the macrophage, infecting adjacent macrophages and repeating this cycle (Natarajan et al., 2020). If able to persist against the innate response, *Mtb* can diffuse to other cell types (Delogu et al., 2013). In the early stages of infection, *Mtb* can disseminate to other organs through the lymphatics system and hematogenous dissemination (Delogu et al., 2013). The primary virulence factor for *Mtb* is its five, type 7 secretion systems,

with the best characterized secretion system being ESX1, which is essential for full virulence (Delogu et al., 2013). ESX1 is used to evade the phagosome of macrophages and translocate into the cytoplasm, where *Mtb* replicates freely, camouflaged by the macrophage (Delogu et al., 2013). The primary protection feature that contributes to the virulence of *Mtb* is its outer membrane, which is particularly defensive against destructive compounds and contributes to drug resistance (Delogu et al., 2013).

There are two types of clinical manifestations of TB infections, pulmonary and extrapulmonary. The most common type of TB infection is pulmonary which results from *Mtb* infecting the alveolar space. Extrapulmonary TB infections (EPTB) affect organ systems outside of the lungs (*e.g.*, brain, kidneys, bones, joints, etc.) and account for about 15-20% of all TB infections (Natarajan et al., 2020). Extrapulmonary infections typically result from a pulmonary infection, developing due to bacteria spreading from the primary site of infection to a secondary organ system through hematogenous dissemination or, less commonly, from poor granuloma formation during both active and latent infections (Al-Sayyad and Abumunaser, 2011). Symptoms of an EPTB infection vary depending on the organ system affected but are predominantly characterized by unexplained weight loss, loss of appetite, night sweats, fever, and fatigue (Centers for Disease Control and Prevention - CDC). An extrapulmonary infection of the bones and joints can lead to osteoarticular tuberculosis (OAT); EPTB infections of the bones and joints make up 10-15% of all EPTB infections and 1-4.3% of all TB infections (Natarajan et al., 2020; Arathi et al., 2013). While *Mtb* can reach the bones and joints through the bloodstream, the bacteria can also infect indirectly through the epiphyseal or metaphyseal spaces (Tuli, 2002). OAT is a monoarticular disease that primarily affects the weight-bearing joints, such as the ankles, hips, and knees, but can also affect the spine and wrists (Al-Sayyad and Abumunaser, 2011). Osteoarticular

TB results in joint swelling, joint effusion, and bone erosion and is characterized by increased bone resorption due to increased osteoclastogenesis.

Diagnosis of OAT is difficult as symptoms are often misdiagnosed as a degenerative disease such as gout or a rheumatic disease such as rheumatoid arthritis (Pigrau-Serrallach and Rodríguez-Pardo, 2013). Early radiological screenings initially show soft tissue swelling, periosteal thickening, and periarticular joint destruction (Pigrau-Serrallach and Rodríguez-Pardo, 2013). Proper diagnosis requires reasonable suspicion of a *Mtb* infection and confirmation by bacterial culture through arthrocentesis or biopsy. (Pigrau-Serrallach and Rodríguez-Pardo, 2013).

Bacterial culture from patient specimens is the only way to definitively diagnose a TB infection, though extrapulmonary infections are difficult to diagnose since infection sites are often inaccessible (Lee, 2015). Diagnosing extrapulmonary infections is primarily done through biopsy and requires histological analysis; diagnostic accuracy can be increased through additional testing such as PCR (Lee, 2015). When the extrapulmonary site is inaccessible for biopsy, physicians will often use body fluid for analysis (Lee, 2015). One of the most widely used biomarkers is the level of adenosine deaminase (ADA); ADA is an enzyme involved in purine metabolism found in many tissues, particularly in T cells (Lee, 2015). The activity of this enzyme is upregulated in T cells during a TB infection due to the presence of mycobacterial antigens (Lee, 2015). Common diagnostic tools used for pulmonary TB infections, such as the tuberculin skin test (TST) or IFN-γ releasing assay (IGRA) may be supportive in the diagnosis of EPTB infections but have limited diagnostic power as they cannot distinguish between active and latent infections, and in countries where BCG vaccination is common, the test can provide false positives (Lee, 2015).

Current Treatments for Osteoarticular Tuberculosis

The current treatment for OAT is the standard treatment of care for all TB infections: a 3-4 multi-antibiotic regimen for 6-12 months with treatment time being dependent on the strain and its severity; the four-drug regimen uses rifampin (RIF), isoniazid (INH), pyrazinamide (PZA), and ethambutol (EMB), these are considered first-line treatments (CDC, 2020; Guillouzouic et al., 2020). This treatment method aims to decrease TB transmission, prevent the emergence of naturally resistant strains, and prevent reinfection (Rabahi et al., 2017). The efficacy of these medications is up to 90%, though disease eradication heavily relies on patient adherence to treatment (Rabahi et al., 2017). The recommended method to ensure treatment adherence is directly observed therapy (DOT) in combination with incentives and enablers for patients; the DOT method requires a trained healthcare professional to administer and watch the patient take their medications as opposed to using at-home self-administration (CDC).

There are four basic treatment regimens recommended for treating adults (CDC, Table 1). All regimens include an initial two-month phase followed by 4–7-month continuation phase; the initial phase is meant to eliminate the majority, if not all, of the bacilli, prevent re-emergence, and determine the future course of treatment, while the continuation phase is meant to eliminate any remaining bacilli (CDC, Table 1). The initial phase focuses on using the first-line antibiotics unless it is known that the infectious strain has antibacterial resistance (CDC). Rifampin is an antibiotic commonly used to treat and prevent mycobacterial infections; it works by inhibiting DNA-dependent RNA polymerase by sterically blocking the path of the elongating RNA at the 5’ end or decreasing the affinity for RNA polymerase to transcribe short transcripts (Suresh et al., 2022). Isoniazid is the most important antibiotic for treating TB; it is a prodrug activated by KatG, a

catalase-peroxidase enzyme that creates a variety of radicals and adducts that inhibit the production of the mycolic acids that make up the mycobacterial cell wall (O'Connor and Brady, 2022).

Additionally, this mechanism of action allows INH to be synergistic with the coinciding treatments (O'Connor and Brady, 2022). The mechanism of action for Pyrazinamide is not fully understood, though it is believed that once PZA is converted to its active form, it can inhibit trans-translation or Coenzyme A synthesis (Padda and Reddy, 2022). Lastly, Ethambutol inhibits arabinosyltransferases and prevents the biosynthesis of the mycobacterial cell wall (Padda and Reddy, 2022).

ELP-004

ELP-004 is a novel compound that has been found to inhibit bone erosion in murine models of arthritis (McCall et al., unpublished). ELP-004 is a methylated derivative of 3,4-dichloroaniline (DCPA), a known antagonist of calcium-release activated calcium (CRAC) channels (Zhou et al., 2011). The core structure of ELP-004 is composed of aniline, which has a high risk of forming reactive metabolites, but is designed to be stabilized through methylation of the amide nitrogen (McCall et al., unpublished). Studies with ELP-004 have shown decreased osteoclast formation and bone erosion in vitro and in vivo using arthritis mouse models with the goal being to treat patients with rheumatoid arthritis (McCall et al., unpublished). Since OAT is characterized by increased osteoclast formation and there is currently no treatment for bone erosion resulting from a TB infection, the efficacy of using ELP-004 to treat bone erosion from a TB infection was assessed in these studies.

Specific Aims

The purpose of this study is to establish a novel treatment for the degradation of bone in osteoarticular tuberculosis patients. Preliminary in vitro studies with RAW264.7 cells show that infection with H37Rv *Mtb* prevents the formation of tartrate-resistant acid phosphatase (TRAP) positive cells. The resulting cells are multi-syncytial, suggesting a blockage in the signaling pathway of TRAP. The signaling pathway from pre-osteoclast to mature osteoclast formation in relation to osteoarticular TB has yet to be defined. While TB is preventable and treatable, late infection detection and increasing occurrence of antibiotic resistance presents an increased challenge for treating future infections. Currently, the only treatment methods for osteoarticular TB and resulting adverse conditions are a 6–12-month round of antibiotics, which neglect to resolve the bone deformities and nerve compression due to increased osteoclastogenesis.

The long-term goal of this study is to inhibit bone erosion by blocking the signaling pathway responsible for inducing overactive osteoclastogenesis in osteoarticular tuberculosis patients using the novel pharmaceutical, ELP-004. To resolve this issue, I will determine the levels of various genes expressed during osteoclast differentiation to define the signaling pathway responsible for creating multi-syncytial cells upon infection with TB. RAW264.7 cells will be differentiated into osteoclast-like and multi-syncytial cells using RANKL or H37Rv *Mtb*. The NFATc1, DC-STAMP, and TRAP expression levels will be compared to RANKL expression to assess the timing of osteoclast and multi-syncytial formation in a TB infection. ELP-004 will be added to RAW264.7 cells following infection by H37Rv *Mtb* to inhibit the differentiation of these cells into their multi-syncytial form. Secondly, I will assess the interactions between the novel pharmaceutical, ELP-004, and two first-line antibiotics, rifampin and isoniazid, using a naive

mouse model. Assessment of interactions will be done using qPCR to observe changes in levels of cytochrome P450 (CYP) expression in the liver and histological changes of the liver and kidneys. The proposed studies will allow for the innovation of the treatment of osteoarticular tuberculosis and provide elevated insight on the mechanism by which patients are experiencing bone deformities and nerve compression. Defining the pathway of osteoclastogenesis and assessing the level of toxicity in this novel treatment for osteoarticular tuberculosis will contribute to furthering treatment and prevention options for patients around the world.

Specific Aim 1: Determine the pathway preventing the activation of TRAP in multi-syncytial cells formed from RAW264.7 cells after inoculation with H37Rv *Mtb* and knockdown multi-syncytial formation using ELP-004.

Hypothesis: Inoculation of RAW264.7 will lead to the formation of multi-syncytial cells activated by markers of osteoclastogenesis which can be knocked down by treatment with ELP-004.

Specific Aim 2: Determine whether there are interactions between the novel compound ELP-004 and first-line antibiotics used to treat tuberculosis infections.

Hypothesis: Combination treatment with ELP-004, rifampin, and isoniazid, will not lead to hepatotoxic effects determined by assessment of the cytochrome p450 system and histological analysis of the livers and kidneys.

Table 6.3
Drug Regimens for Pulmonary TB in Adults Caused by Drug-Susceptible Organisms*

Initial Phase			Continuation Phase			
Regimen	**Drugs**	**Interval and Doses± §**	**Regimen**	**Drugs**	**Interval and Doses± §**	**Range of Total Doses**
1	**INH RIF PZA EMB**	7 days/week for 56 doses (8 weeks) **or** 5 days /week for 40 doses (8 weeks)¶	**1a**	**INH RIF**	7 days/week for 126 doses (18 weeks) **or** 5 days/week for 90 doses (18 weeks)	182–130 (26 weeks)
			1b#	**INH RIF**	2 days/week for 36 doses (18 weeks)	92–76 (26 weeks)
			1c**	**INH RPT**	1 day/week for 18 doses (18 weeks)¶	74–58 (26 weeks)
2	**INH RIF PZA EMB**	7 days/week for 14 doses (2 weeks), then 2 days/ week for 12 doses (6 weeks) **or** 5 days/week for 10 doses (2 weeks),¶ then 2 days/week for 12 doses (6 weeks)	**2a#**	**INH RIF**	2 days/week for 36 doses (18 weeks)¶	62–58 (26 weeks)
			2b**	**INH RPT**	1 day/week for 18 doses (18 weeks)¶	44–40 (26 weeks)
3	**INH RIF PZA EMB**	3 times weekly for 24 doses (8 weeks)	**3a**	**INH RIF**	3 times weekly for 54 doses (18 weeks)¶	78 (26 weeks)
4	**INH RIF EMB**	7 days/week for 56 doses (8 weeks) **or** 5 days/week for 40 doses (8 weeks)¶	4a	**INH RIF**	7 days/week for 217 doses (31 weeks) **or** 5 days/week for 155 doses (31 weeks)¶	273–195 (39 weeks)
			4b#	**INH RIF**	Twice weekly for 62 doses (31 weeks)¶	118–102 (39 weeks)

INH = isoniazid RIF = rifampin PZA = pyrazinamide EMB = ethambutol RPT = rifapentine

* For more information on strength of recommendation and quality of supporting evidence, refer to treatment of tuberculosis guidelines. *MMWR* 2003; 52 (No.RR-11).

± When DOT is used, drugs may be given 5 days/week and the necessary doses adjusted accordingly.

§ Patients with cavitation on initial chest x-ray and positive cultures at completion of 2 months of therapy should receive a 7-month continuation phase.

¶ Patients on regimens given less than 7 days a week should receive DOT.

Regimens given less than 3 times a week are **not** recommended for HIV-infected patients with CD4+ counts less than 100

** Used only for HIV-negative patients with negative sputum smears at completion of 2 months of therapy and who do **not** have cavitation on initial chest x-ray. For patients started on this regimen and found to have positive culture from the 2-month specimen, treatment should be extended an extra 3 months.

Table 1. Drug Regimens for Pulmonary TB in Adults (CDC).

Chapter 2

Assessing the Effect of H37Rv *Mtb* on RAW264.7 Cells

Introduction

Osteoclastogenesis

Bone is a connective tissue that is essential for movement and metabolic function; bone provides mechanical support for motion, protection for vital organs, hosts a major reserve of calcium and phosphate to maintain mineral homeostasis, and may assist in the regulation of energy expenditure (Xu and Teitelbaum, 2013). Bone is dynamic, and in normal homeostasis, a cycle of building and degrading bone proceeds reciprocally to ensure no net change in bone mass. Bone homeostasis is regulated by the basic multicellular unit (BMU); the adult human skeleton contains about 1-2 million BMUs that are spatially and temporally separated and function asynchronously (Xu and Teitelbaum, 2013). The BMU is made up of four cell types: bone lining cells, osteocytes, osteoclasts, and osteoblasts (Xu and Teitelbaum, 2013). Bone lining cells form the quiescent monolayer on the bone surface, osteocytes are the primary mechanosensing cell and regulate the activation of bone remodeling, osteoclasts are responsible for the resorption of old bone, and osteoblasts are responsible for the formation of new bone (Xu and Teitelbaum, 2013). Osteoclastogenesis defines the formation of osteoclasts from the monocyte-macrophage lineage. Osteoclasts are multinucleated, giant cells that form through cell-cell interactions (Kodama and Kaito, 2020). Bone erosion occurs when there is a dysregulation in the homeostatic BMU cycle, resulting in increased osteoclast production (Xu and Teitelbaum, 2013). OAT is characterized by this dysfunction, leading to the degradation of the bones and joints.

Osteoclasts are developed from monocytes in a complex pathway involving colony stimulating factor-1 (CSF-1) and receptor activator of nuclear factor kappa-B ligand (RANKL), which are presented by osteoblasts and osteocytes (Kodama and Kaito, 2020). RANKL and CSF-1 bind to their receptors, RANK and CSF-1R respectively, to activate a series of downstream signaling pathways, one of which involves tumor necrosis factor receptor-associated factor-6 (TRAF6) (Zhao, 2009). The activation of TRAF6 is followed by activation of nuclear factor-kappa B (NF-kB) (Zhao, 2009). NF-kB is a pleiotropic transcription factor necessary for the regulation of osteoclast production, function, and survival (Soysa and Alles, 2009). NF-kB cooperates with nuclear factor of activated T-cells cytoplasmic-2 (NFATc2) to initiate the induction of NFATc1, a regulator of cell fate determination (Zhao, 2009). The finalizing factor in the production of mature osteoclasts is the binding of calcium (Ca^{2+}). Calcium dephosphorylates NFATc1 allowing NFATc1 to translocate into the nucleus from the cytoplasm (Zhao, 2009). Calcium enters the cytoplasm through the Orai-1 channel. Orai-1 is a calcium membrane channel that is responsible for the influx of extracellular calcium into the cell upon the depletion of internal calcium stores (Putney, 2009). Without calcium, NFATc1 is unable to dephosphorylate, preventing the differentiation of osteoclasts.

Osteoclastogenesis can be assessed in vitro through a tartrate-resistant acid phosphatase (TRAP) stain. The TRAP enzyme is regulated by the *ACP5* gene, which often codes for the TRAP5b isoform in relation to osteoclast formation (U.S National Library of Medicine). TRAP is primarily responsible for regulating osteopontin, a protein produced by osteoclasts and some immune cells (MedlinePlus, 2013). During remodeling, osteopontin is activated, allowing the osteoclasts to bind to the bone and begin the resorption process; once resorption is complete, osteopontin is deactivated and osteoclasts are released from the bone surface (MedlinePlus, 2013).

This upregulation of TRAP expression during differentiation allows it to be used as a histochemical marker for the assessment of osteoclast differentiation. Osteoclast formation can also be assessed in vitro using an osteo assay. The Corning osteo assay plate contains a synthetic surface made of inorganic crystalline calcium phosphate, mimicking a living bone material (Rao et al.). These plates allow for the assessment of osteoclast formation through pit development; the osteoclasts stick to the surface and resorb the synthetic bone forming pits (Rao et al.). Pit formation can be assessed through the use of microscopy.

RAW264.7 Cells

RAW264.7 cells (ATCC, TIB-71) are a murine monocyte/macrophage cell line established from a tumor in a male BALB/c mouse immortalized with Abelson murine leukemia virus (ATCC). These cells are designated as an adherent cell line and function as a monolayer but can also contain some suspended populations (ATCC). Common morphological features include adherent cuboidal, spindle-shaped, or rounded cells if viable (ATCC). RAW264.7 cells are capable of performing functions of macrophages including phagocytosis, pinocytosis, target cell killing through antibody dependent cytotoxicity, and differentiation into osteoclast-like cells through stimulation with RANKL (Taciak et al., 2018). RANKL-induced osteoclast-like formation in RAW264.7 cells is a widely used in vitro model for studying osteoclastogenesis and bone resorptive diseases and conditions due to its ability to resorb bone in vitro (Kong et al., 2019).

TNF-α Aids in the Progression and Protection Against *Mtb* Infections

Tumor necrosis factor α (TNF-α) is protective and pathogenic when it comes to TB infections (Dorhoi and Kaufmann, 2014). The presence of TNF-α at the time of infection can make the difference between life or death, giving TNF-α a dual functionality (Dorhoi and Kaufmann, 2014). Previous research has shown that patients taking TNF-α blockers have an increased risk for susceptibility and death from a TB infection; this is because TNF-α is responsible for eliciting proinflammatory functions and low or zero abundance of TNF-α results in decreased macrophage responses and poor granuloma formation (Dorhoi and Kaufmann, 2014). In contrast, an excess of TNF-α can interfere with natural cell death processes, resulting in hyperinflammatory responses (Dorhoi and Kaufmann, 2014).

Apoptosis is a form of natural cell death that is regulated by a variety of mechanisms. The progression of OAT is furthered when cells transition from apoptotic cell death to autophagic cell death (Liu et al., 2020). Previous research has shown that when cells are pre-treated with TNF-α, it pushes them towards autophagy as opposed to apoptosis (Liu et al., 2020). Once *Mtb* enters the bones, there is an influx on TNF-α production from mononuclear macrophages; here, TNF-α acts directly on osteoclast precursors, leading to increased osteoclast production (Liu et al., 2020). The duality of TNF-α allows it to prevent and aid in the fight against TB infections while also promoting and causing bone degradation through osteoclasts.

Methods

Culturing RAW 264. 7 Cells

Frozen RAW264.7 cells (ATCC, TIB-71) were rapidly thawed at 37℃ in a water bath and resuspended in 10 mL of Dulbecco's Modified Eagle Medium (DMEM, Corning, 15-013-CV) containing 4.0 mM of L-glutamine, 1.5 g/L of sodium bicarbonate, 4.5 g/L of glucose, 1.0 mM of sodium pyruvate, 1X penicillin/streptomycin, and 10% fetal bovine serum for growth. The cells were spun down at 4℃ for 5 minutes at 500 relative centrifugal field (RCF) and the supernatant was removed. The cells were resuspended a second time in 10 mL of DMEM. The cells were plated and grown on a tissue culture-treated petri dish at 37℃ with 5% CO_2. To subculture confluent cells, the cells were scraped using a rubber-tipped scraper and added to fresh media; the dilution was based on confluency. Cells were thrown out following passage 15.

Osteoclast-Like Differentiation using RAW264.7 Cells

RAW264.7 cells were scraped using a rubber-tipped cell scraper and spun down at 4℃ for 5 minutes at 500 RCF. The old media was removed, and the cells were resuspended in 5 mL of Minimum Essential Medium, Alpha (α-MEM, Corning, 15-012-CV) containing 2.0 mM of L-glutamine, 1X penicillin/streptomycin, and 10% fetal bovine serum. Cells were mixed with trypan blue at dilutions based on confluency and counted using a hemocytometer. Cells (0.25 mL) were plated at 12 x 10^3 cells/mL in a tissue culture-treated 24-well plate. Cells were supplemented with 0.25 mL of additional media (control), 100 ng/mL of RANKL (ATCC, 200-04), or 25 μg/mL of H37Rv *Mtb* lysate (ATCC, NR-14822). Every 2-3 days, the media was removed from the wells and replaced with fresh α-MEM; each well received 0.5 mL of fresh media (control) or fresh media supplemented with RANKL or H37Rv *Mtb*.

Tartrate-Resistant Acid Phosphatase (TRAP) Staining

Following 5, 7, or 10 days of osteoclast-like differentiation, RAW264.7 cells were TRAP stained to detect osteoclast-like cell formation; all staining was performed using the Leukocyte Acid Phosphatase (TRAP) kit by Sigma-Aldrich (SLC0817). The TRAP kit was brought to room temperature for an hour. An aliquot and tray of DI water were warmed in the water bath and the incubator at 37℃, respectively. A fixative solution and beaker B solution, the tartrate-resistant stain, was made using the components and concentrations found in Table 2. The media was aspirated from the wells and 0.5 mL of Fixative solution was added to each well and incubated at room temperature for 10 minutes. The Fixative solution was aspirated from the wells and each well was gently washed with 1 mL of warmed DI water to prevent cells from dislodging from the well surface. The DI water was aspirated from the wells and 0.5 mL of Beaker B solution was added to the wells. The plate was incubated in a DI water bath in the incubator for 1 hour at 37℃ with 5% CO_2. The Beaker B solution was aspirated from the wells and the plate was left to dry overnight. Assessment of TRAP activity was performed using microscopy. TRAP-positive staining is indicated by a purple-red stain and TRAP-negative staining a yellow color.

Apoptosis and Necrosis Assay

RAW264.7 cells were differentiated for 5 days following the RAW264.7 osteoclast-like differentiation. On a 24-well plate, 6 wells were used for each treatment group; one well from each group was used in the untreated (U), FITC Annexin V only (A), and Propidium Iodide only (PI) control stains. Three wells from each treatment group were used to assess apoptosis and necrosis. All staining was done using the FITC Annexin V Apoptosis Detection Kit 1 from BD Pharmingen (556547). Aliquots of 10 mL of TrypLE Express (Gibco, 12604-013) and 54 mL of Dulbecco's

Phosphate Buffered Saline (DPBS, Corning, 25-055-CV) was warmed in the water bath at 37℃ for 30 minutes. Additionally, a separate 10 mL aliquot of DPBS was placed on ice. The media was aspirated from the wells, then washed once with 0.5 mL of warmed DPBS. The DPBS was aspirated from the wells, replaced with 0.5 mL of TrypLE Express, and the plate incubated for 20 minutes at 37℃ with 5% CO_2. The cells were gently pipetted from the plate and placed into 15 mL conical vials. Pre-warmed DPBS (7.5 mL) was added to each tube, the tubes were centrifuged for 5 minutes at 4℃ at 300 RCF, then the supernatant was removed. The cells were washed twice with 0.25 mL of ice cold DPBS, centrifuged for 5 minutes at 4℃ at 300 RCF, and the supernatant removed. The cells were resuspended in 100 µL of 1x staining buffer (1 mL of 10X Annexin V Binding Buffer (BD Pharmingen, 51-66121E) and 9 mL of cell culture grade water (Corning, 25-055-CV). Following this, the PI and Annexin V only stains were boiled on a heating block at 96℃ for 1 minute. All cells were transferred to appropriately labeled FACS tubes. No stain was added to the U tube, 5 µL of propidium iodide solution (BD Pharmingen, 51-66211E) was added to the PI only tube, 5 µL of FITC Annexin V (BD Pharmingen, 51-65874X) was added to the the Annexin only tube, and 5 µL of both the propidium iodide solution and FITC Annexin V were added to all sample tubes (Control, RANKL, and H37Rv *Mtb* only tubes). Each tube was gently vortexed (setting 4) and incubated at room temperature for 15 minutes in the dark. Lastly, 0.4 mL of the 1x staining buffer was added to each tube, and the cells were analyzed using flow cytometry within an hour. All flow cytometry was conducted using a BD LSRFortessa.

Corning Osteo Assay

RAW264.7 cells were differentiated for osteoclast-like cells in a 24-well Corning Osteo Assay Plate (20-031-CV); the cells were differentiated at 7 and 10 days. Additionally, all groups were treated with ELP-004 at concentrations of 200, 100, 50, and 25 µM. Following 7 or 10 days of differentiation, the media was aspirated from the wells and replaced with 10% bleach for 5 minutes. The wells were then washed 3 times with DI water and left overnight to dry. Assessment of pit formation and cell mobility was performed using the Lionheart Live Cell Imaging System (Agilent BioTek) at 20x phase contrast. All images were processed and analyzed using Fiji ImageJ software.

qPCR Analysis of RAW264.7 cells

RAW264.7 cells were differentiated for osteoclast-like formation for four days as described above. On days 3 and 4, 1 mL of TRIzol (Invitrogen, 15596036) was used to isolate RNA from the wells. Chloroform (0.2 mL) was added to each tube, vortexed, and incubated for 3 minutes. The samples were then centrifuged for 15 minutes at 12,000 RCF at 4°C. The aqueous phase was transferred to another eppendorf tube and 1 µL of GlycoBlue (Invitrogen, AM9515) was added to each tube; the phenol-chloroform phase was discarded. Following this, 0.5 mL of isopropanol was added to the aqueous phase and incubated overnight at -20°C. The samples were vortexed and pulse spun following overnight incubation at -20°C. The samples were centrifuged for 10 minutes at 12,000 RCF at 4°C and supernatant was removed. The pellet was resuspended in 1 mL of 75% ethanol, vortexed briefly, and then centrifuged for 5 minutes at 7600 RCF at 4°C. The supernatant was discarded, and the pellets were left to air dry for 10 minutes. The pellets were resuspended in 44 µL of RNase-free water and frozen at -80°C. The samples were thawed and a

DNase treatment was conducted using the DNA-*free* Kit by Ambion (AM1906) as instructed in the kit. Concentrations of RNA were assessed using a Nanodrop. RNA used in the cDNA reaction was normalized to a volume of 500 ng per sample. The cDNA synthesis reaction was carried out using the iScript cDNA Synthesis Kit from Bio-Rad (cat. 1708890) for a volume of 40 µL. Amplification of the genes was carried out by using the Applied Biosystems GeneAmp PCR System 9700. The cDNA samples were frozen at -20℃ prior to qPCR analysis. The cDNA, primers, and SYBR Green Supermix (Bio-Rad, 1725274), were thawed over ice. cDNA (2 µL) was placed in triplicate into Bio-Rad Hard Shell qPCR plates followed by 18 µL of master mix (SYBR Green Supermix + primers). The microplate was sealed using Seal Type B and a flat white rubber card to ensure complete seal of each well. The plate was vortexed briefly, then centrifuged for 1 minute at 300 RCF. Plates were analyzed using the Bio-Rad CFX OPUS Real-Time PCR System. Expression of target genes was normalized to HPRT and β-Actin expression.

TNF-α RAW264.7 Cell Experiment

RAW264.7 cells were plated at a concentration of 12 x 10^4 cells/mL in a tissue culture-treated 24 well plate resuspended in 250 µL of α-MEM. Two hours following the initial plating, the cells received additional media supplemented with 100 ng/mL of RANKL or 40 ng/mL of TNF-α (Abcam, P06804). On day 2, 100 µL of H37Rv *Mtb* (6.25 µg/mL or 25 µg/mL) in α-MEM were added to the wells containing TNF-α. 2 hours following the addition of H37Rv *Mtb,* TNF-α + *Mtb* wells were treated with 200, 100, 50, 25 µM of ELP-004. The cells were refed and retreated every 3 days. Assessment of osteoclast differentiation was performed at days 7 and 10 using a TRAP stain and Corning Osteo Assay.

Results

RAW264.7 cells exposed to H37Rv *Mtb* do not form TRAP-positive syncytial formations

To determine the effect of H37Rv *Mtb* on osteoclast-like formation in RAW264.7 cells, RAW264.7 cells were incubated with either RANKL (100 ng/mL) or H37Rv *Mtb* (25 µg/mL) for 5, 7, or 10 days to result in osteoclast-like differentiation (Fig. 1). Assessment of osteoclast-like cell differentiation was done by performing a TRAP stain; positive TRAP staining is indicated by a red-purple stain while negative staining is indicated by yellow staining. Even at several time points, cells exposed to H37Tv *Mtb* resulted in negative TRAP staining, though the cells did become multi-syncytial; cells exposed to H37Rv *Mtb* did not form large multinucleations as shown in the RANKL cells (Fig. 1). Qualitative analysis of the wells also showed increased cellular debris and dead cells in the H37Rv *Mtb* wells by day 5 with the level of debris increasing with longer timepoints (Fig. 1) From this it was concluded that a 5-day time-point was most ideal for TRAP staining, though 10 days may provide the necessary time for multinucleation to complete.

RAW264.7 cells inoculated with H37Rv *Mtb* have increased apoptotic cell death

Since TRAP stains of RAW264.7 cells exposed to H37Rv *Mtb* show increased cellular debris compared to the control and RANKL-treated cells, flow cytometry was used to assess and

compare cell death among the experimental groups. Compared to the control and RANKL wells, there was significantly increased early in RAW264.7 cells exposed to *Mtb* (Fig. 2). Compared to the RANKL wells, there were significantly fewer live cells and significantly more late apoptotic cells among the H37Rv *Mtb* exposed cells (Fig. 2). From this data, it was concluded that the concentration of H37Rv *Mtb* was too high, resulting in increased apoptotic cell death. From here, the concentration of *Mtb* used was reevaluated.

RAW264.7 cells do not mobilize bone when exposed to H37Rv *Mtb*

To determine whether syncytial cells induced by H37Rv *Mtb* were functional osteoclast-like cells, RAW264.7 cells treated with 100 ng/mL of RANKL or 25 μg/mL of H37Rv *Mtb* were plated in an osteo assay plate and simultaneously treated with varying concentrations of ELP-004 for 5 days and pit formation was quantified. It was determined that 5 days was not long enough to observe resorption in the osteo assay plates. Although pit resorption was low at the 5-day time point, compared to RANKL cells, cells exposed to H37Rv *Mtb* could not mobilize bone in the same capacity. Considering the possibility that H37Rv *Mtb* could not produce osteoclast-like cells alone, an additional osteo assay was conducted with wells that contained a combination of RANKL and H37Rv *Mtb* for 7 and 10 days. A second identical plate was set up to observe TRAP formation. Cells were treated with a combination of 100 ng/mL of RANKL and 25 μg/mL of H37Rv *Mtb*. At day 7, TRAP staining and osteo assay analysis showed poor multinucleation of the cells. The TRAP stain results showed two distinct populations of cells. However, no larger osteoclast-like cells were seen as a result of the combination of RANKL and H37Rv *Mtb* at 7 and 10 days (Fig. 3a). Additionally, the combination treatment did not increase cell mobilization (Fig. 3b). Treatment with ELP-004 had a concentration-dependent elimination of syncytial formation in the

combination treatment at both 7 and 10 days (Fig. 3a and 3b). These data confirmed what was observed with previous TRAP assays. It was therefore concluded that there may be a blockage in the pathway associated with the differentiation of monocytes into osteoclasts since multinucleation was still occurring.

Acp5 (TRAP), *Nfatc1*, and *Dc-stamp* are not expressed in RAW264.7 cells exposed to H37Rv *Mtb*

Previous data showed that exposing RAW264.7 cells to *Mtb* does not result in TRAP-positive cell formation. To determine whether there is a transcriptional blockage in the differentiation pathway of monocytes to osteoclasts, RNA was isolated from RAW264.7 cells on days 3 and 4 following osteoclast-like differentiation (Lampiasi et al., 2021). Markers associated with osteoclast differentiation were significantly upregulated in cells isolated from RANKL wells (Fig. 4). Cells isolated from H37Rv *Mtb* exposed wells showed little expression which was comparable to the negative control (Fig. 4). From this it can be concluded that while multinucleation was occurring as a result of exposure to H37Rv *Mtb*, the cells cannot be classified as osteoclast-like.

Incubation with TNF-α does not change the functionality or expression of RAW264.7 cells in vitro

Previous studies have indicated the importance of TNF-α in bone erosion (Liu et al., 2020; Xiao and Xiao, 2019). Here, RAW264.7 cells were pre-treated with 40 ng/mL of TNF-α in an effort to promote autophagy, a necessary mechanism in the promotion of bone erosion (Liu et al., 2020; Xiao and Xiao, 2019). RAW264.7 cells were differentiated into osteoclast-like cells by

pretreatment with TNF-α H37Rv (40 ng/mL) and *Mtb* (6.25 or 25 μg/mL) or RANKL (100 ng/mL) for 5 or 10 days. Additionally, cells exposed to H37Rv *Mtb* and TNF-α were also treated with 25, 50, 100, or 200 μM of ELP-004. RAW264.7 cells exposed to H37Rv *Mtb* had decreased cell death and debris in wells at a concentration of 6.25 μg/mL compared with wells at 25 μg/mL (Fig. 5a and 5b). Additionally, larger multinucleated cells were formed in cells exposed to 6.25 μg/mL H37Rv *Mtb* compared to 25 μg/mL when pre-treated with TNF-α (Fig. 5a). There was no change in TRAP staining or pit resorption with the addition of TNF-α at both 5 and 10 days of differentiation. Although there were some residual TRAP staining in cells pretreated with TNF-α, these cells cannot be definitively classified as osteoclast-like cells.

Discussion

RAW264.7 cells are a mouse monocyte/macrophage cell line that are commonly used in the assessment of osteoclastogenesis in vitro. They can perform the functions of macrophages and upon stimulation with RANKL, can be differentiated into osteoclast-like cells (Taciak et al., 2018). The goal of these experiments was to determine a model for studying tuberculosis infections in vitro and assess the functionality of syncytial cells formed from tuberculosis exposure. Repeated TRAP stains showed no indication of TRAP-positive cell formations in RAW264.7 cells exposed to H37Rv *Mtb,* though multi-syncytial formations still occurred. This result was unexpected as previous literature has established that there is increased osteoclastogenesis upon exposure to TB. Since confluency is important in cell-cell fusion, and increased cellular death and debris was observed in wells containing H37Rv *Mtb*, an apoptosis and necrosis assay was performed, which found significantly increased early apoptosis in RAW264.7 cells exposed to TB. This was to be

expected as cells infected with TB commonly undergo apoptotic cell death. The concern that the decreased cell-cell fusion was due to the significant decrease in live cells in TB exposed wells. Since decreased cell-cell fusion, increased cell death, and no TRAP-positive staining occurred, the functionality of cells exposed to TB was determined using an osteo assay plate. Pit formation rarely occurred in wells containing H37Rv *Mtb.* Although the data was quantified, the analysis program cannot differentiate cell debris from pit formation, making it difficult to assess the true functionality of these cells using these plates. Due to the limitations of the osteo assay plate, the functionality of RAW264.7 cells exposed to H37Rv *Mtb* was assessed by measuring markers upregulated during osteoclast differentiation. It was found that only RANKL-treated cells expressed these markers, confirming previous in vitro work. A continued literature review prompted the use of TNF-α due to its dual functionality in the pathogenesis of TB infections (Dorhoi and Kaufmann, 2014). Pre-treating RAW264.7 cells with TNF-α did not result in changes in TRAP staining or mobilization of bone in cells exposed to TB. Use of the novel compound, ELP-004, throughout these experiments continuously showed a knockdown of either osteoclast-like formation in RANKL-treated cells or multi-syncytial formations in H37Rv *Mtb*-exposed cells. This suggests that although exposure of RAW264.7 cells to *Mtb* alone does not result in osteoclast-like differentiation, there is a potential for the use of ELP-004 in the treatment of patients with OAT.

Likely, the model used to observe osteoclast function in vitro was not the best model. Previous literature has shown that exposure of monocytes to TB leads to osteoclast differentiation, though these experiments use primary monocytes isolated from humans and mice. Although RAW264.7 cells function very similarly to primary monocytes, they may be missing additional functionality that primary monocytes contain, that would allow them to differentiate into

osteoclasts following TB infection. Additionally, previous researchers used live TB instead of an extract for their infection model. Although the H37Rv *Mtb* strain is common with in vitro work, it is often cultured and used directly on primary monocytes.

The inefficiency of this model and time constraints prevented the continuation of this Aim. Future experiments would involve the reworking of this in vitro model with the hopes that osteoclast-formation would occur as a result of a TB infection.

Figures and Table 2

Fixative	Concentration or Percentage Used in Mixture
Citrate	105.84 mM
Acetone	3.77 M
Formaldehyde	8.1%
Beaker B	
DI Water	90.9%
Tartrate	16.58 mol
Fast Garnet GBC Base Solution	0.14 mg/mL
Sodium Nitrate	4.95 M
Naphthol AS-BI Phosphoric Acid Solution	1.23 g/mL
Acetate	6.19 M

Table 2. Concentrations and percentages of components used to make fixative and beaker B for the TRAP stain. The Fast Garnet GBC Base Solution and sodium nitrate were mixed 1:1 before being added to beaker B mixture.

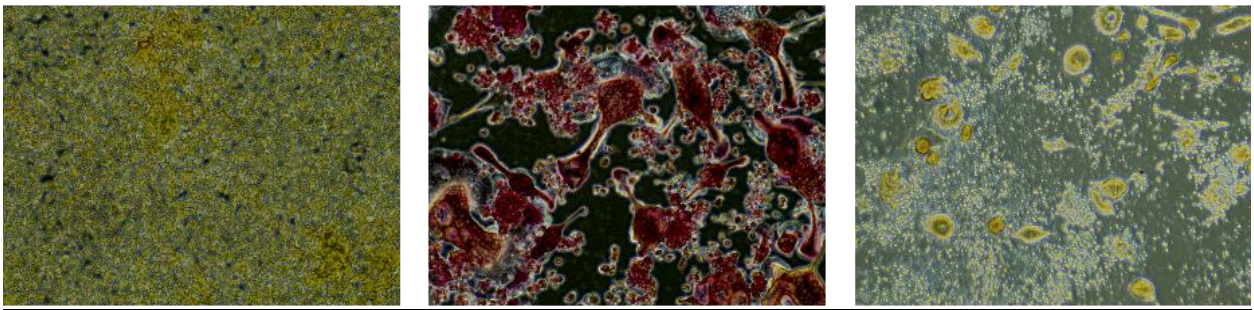

Figure 1. Assessment of osteoclast-like formation at 5 days using a TRAP stain. Control (left), RANKL (middle), H37Rv *Mtb* (right).

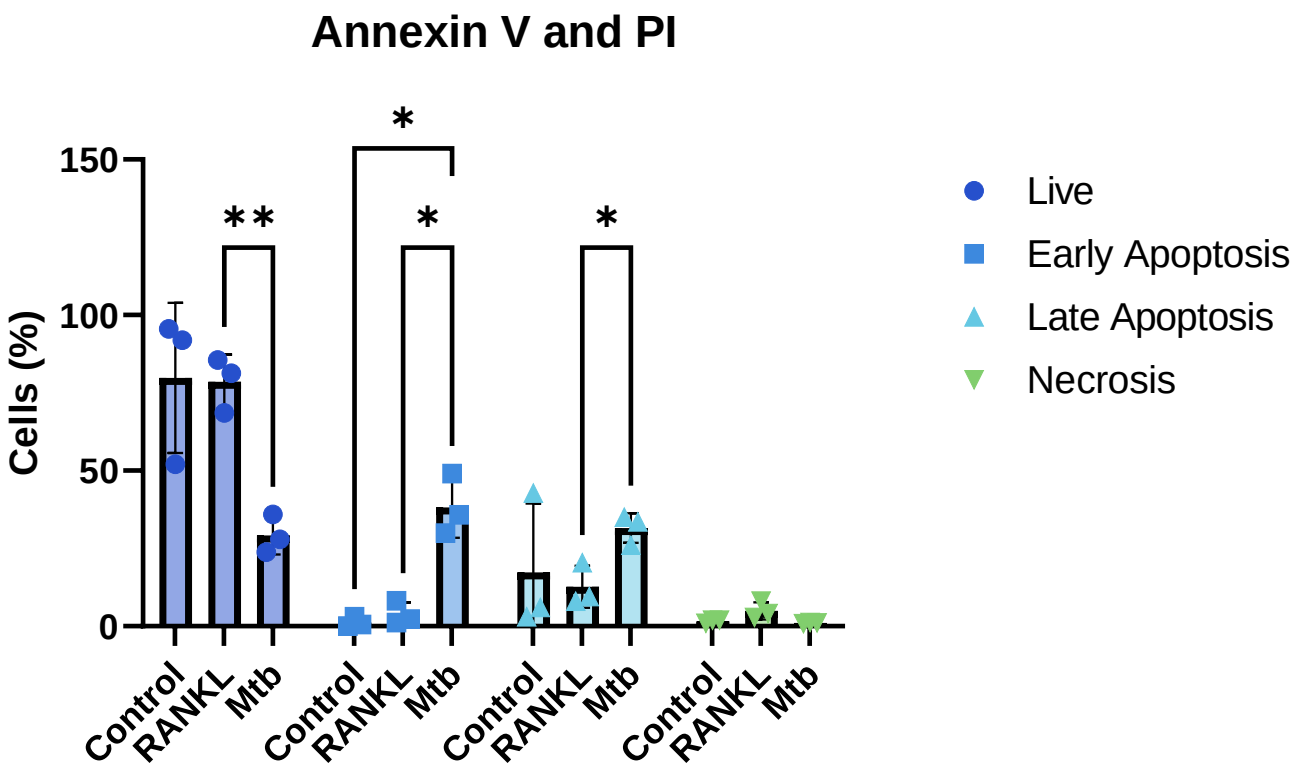

Figure 2. Assessment of apoptosis and necrosis using a FITC and Annexin V stain in RAW264.7 cells differentiated into osteoclast-like cells using RANKL and H37Rv *Mtb*.

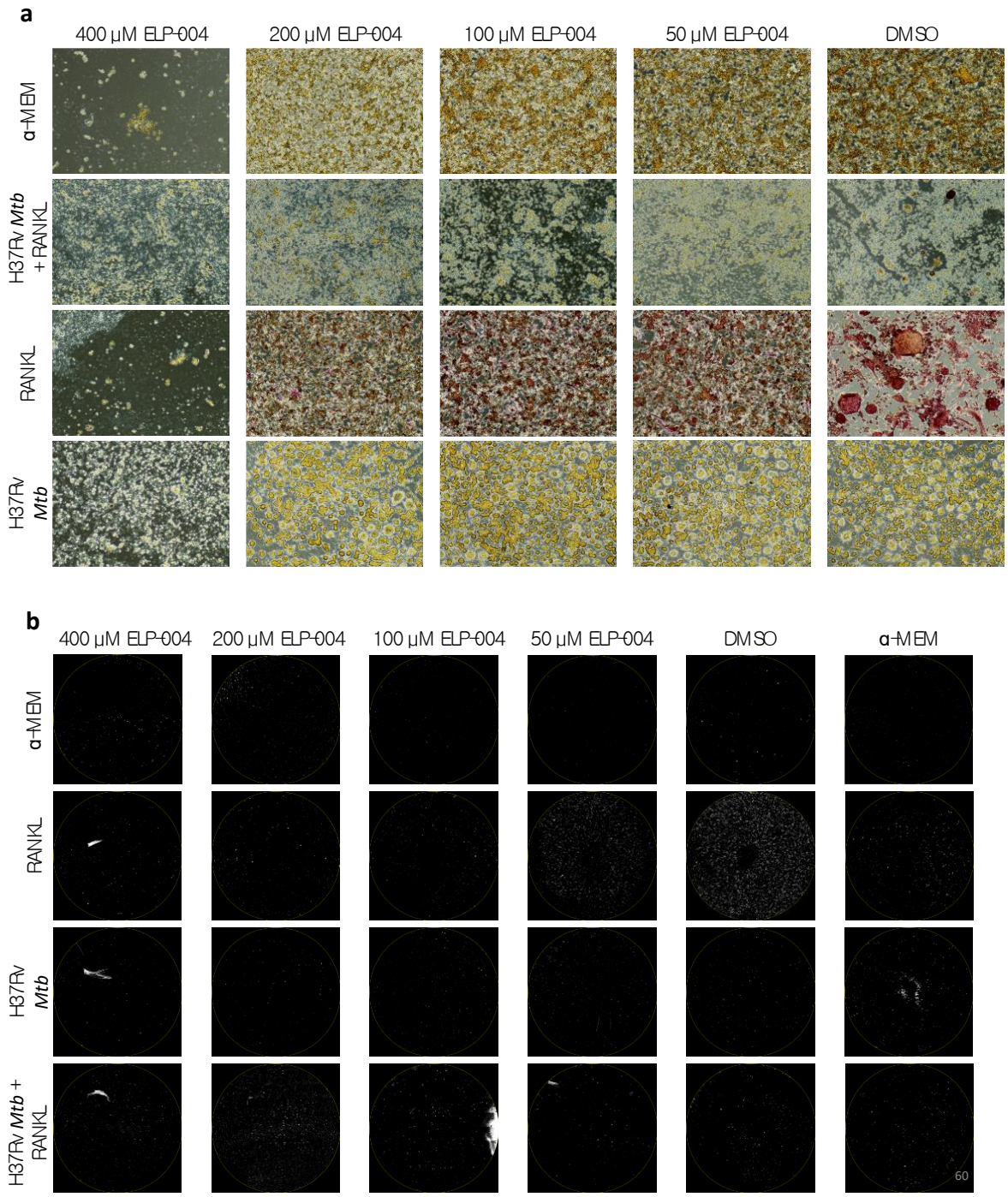

Figure 3. Results from TRAP stain and osteo assay plate at day 10 following differentiation of RAW264.7 cells into osteoclast like cells using RANKL, H37Rv *Mtb*, and a combination of RANKL and H37Rv *Mtb*. White dots on osteo assay plate represent pits formed in the bone matrix.

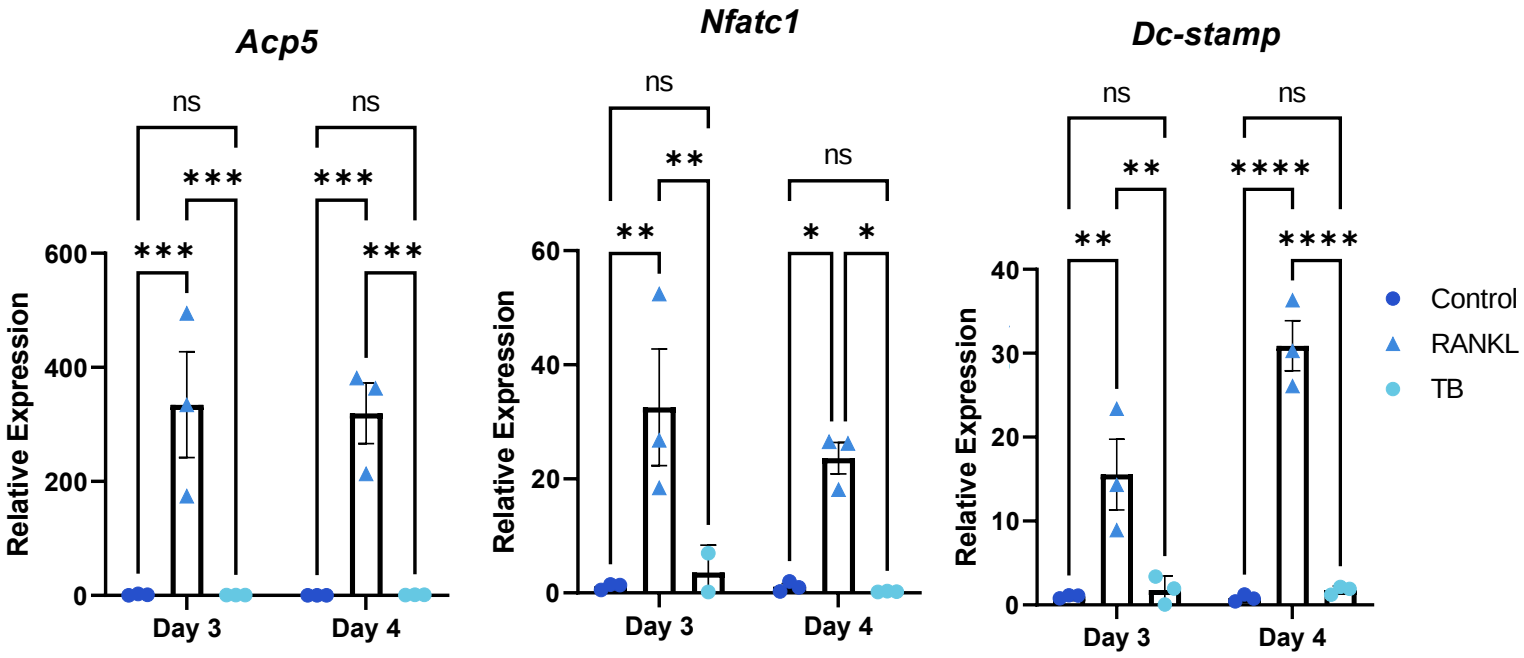

Figure 4. qPCR analysis of *Acp5*, *Nfatc1*, and *Dc-stamp*, markers associated with osteoclast formation.

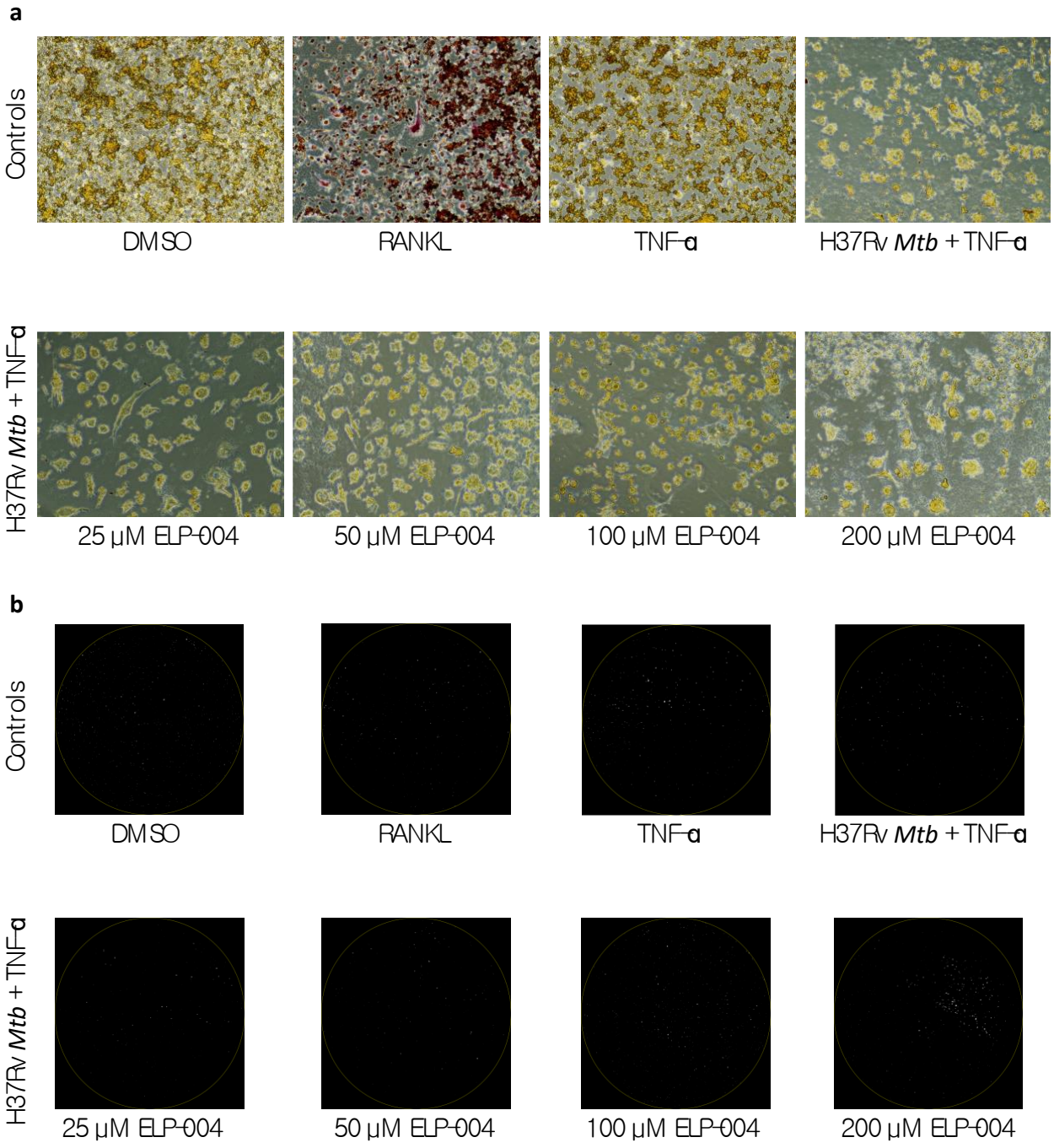

Figure 5. Cells were differentiated into osteoclast-like cells using RANKL or H37Rv *Mtb*. (a) TRAP stain results of RAW264.7 cells pre-treated with TNF-α. (b) Osteo assay results of RAW cells pre-treated with TNF-α.

Chapter 3

Determining the Efficacy of ELP-004 to Be Used in Combination with First-Line Antibiotics

Introduction

Cytochrome P450

The cytochrome P450 (CYP) system contains a series of hemeproteins that are responsible for the metabolism of a variety of drugs and xenobiotics (McDonnell and Dang, 2013). This metabolism of drugs and xenobiotics occurs in a variety of locations in the body including the kidneys, intestinal wall, lungs, plasma, and primarily, in the liver (McDonnell and Dang, 2013). There are more than 50 CYP enzymes, with the most common being: CYP1A2, CYP2C9, CYP2C19, CYP2D6, CYP3A4, and CYP3A5. These enzymes metabolize 90% of all drugs (Lynch and Price, 2007). Foreign molecules are metabolized in phase I and phase II interactions, with phase I interactions being the primary method of metabolism. Phase I metabolism is driven by the CYP system (McDonnell and Dang, 2013).

CYP pathways are classified by the similarities between their gene sequences, and drugs that share a common pathway have the potential for drug-drug interactions (McDonnell and Dang, 2013). Drugs can interact with the CYP system in a variety of ways. Drugs can be metabolized, induce, or inhibit one or multiple CYP enzymes (Lynch and Price, 2007). It is imperative when prescribing CYP inducers or inhibitors, that other prescribed medications considered as the drug-drug interactions can result in decreased efficacy of those medications. Drugs or dosages may need to be adjusted to ensure proper treatment (Lynch and Price, 2007).

First-line antibiotics used to treat tuberculosis are known to be metabolized by CYP enzymes. It is important that liver function is monitored when taking these first-line antibiotics, as all can produce hepatotoxic effects (Padda and Reddy, 2022). The use of rifampin requires

monitoring through complete blood counts (CBC), as it can result in thrombocytopenia and neutropenia. Additionally, rifampin is a potent inducer of CYP3A4, CYP3A5, CYP1A2, CYP2C9, and CYP2C19, which can result in increased metabolism of drugs that follow the same enzymatic pathway (McDonnell and Dang, 2013; Lynch and Price, 2007). Isoniazid can lead to peripheral hepatotoxicity due to pyridoxine deficiency and is a potent inhibitor of CYP2C19, although this can be prevented through the use of B6 supplements (Padda and Reddy, 2022; Lynch and Price, 2007). Pyrazinamide (PZA) can increase uric acid concentrations (Padda and Reddy, 2022) because PZA is primarily metabolized by amidase in the liver and then further metabolized by xanthine oxidase. PZA and its metabolites are mainly excreted by the kidney (Hussain et al., 2021). Ethambutol is metabolized by alcohol dehydrogenase in the liver with 50-70% being excreted by the kidney (Sundell et al., 2020).

Metabolism of ELP-004

ELP-004 is a novel compound whose original purpose serves to eliminate bone erosion in arthritis patients. Although the core structure of ELP-004 can be metabolized into toxic metabolites, methylation of the amide nitrogen prevents the formation of these toxic metabolites and improves its metabolic stability (McCall et al., unpublished). Previous studies in vitro studies show that ELP-004 is primarily metabolized by CYP1A2 and CYP2B6 (McCall et al., unpublished). CYP3A4, an enzyme that metabolizes about 50% of all drugs, is not induced by treatment with ELP-004 (McCall et al., unpublished) In hopes of expanding its usage, these experiments assessed whether there are interactions between ELP-004 and two first-line antibiotics, rifampin and isoniazid, currently used as treatments for OAT.

Methods

Mouse Model for TB Induction

Tuberculosis infection studies were conducted in accordance with guidelines established by West Virginia University's Office of Lab Animal Resources. Protocols were approved by the local Institutional Animal Care and Use Committee (protocol: 1709009365). 7-week-old female C3H/HeJ and C57BL/6J (n = 16) were infected with 800 colony-forming units (CFU) of *Mtb* intranasally; 2 mice were used as uninfected controls for each group. Animals were purchased from the Jackson Lab (strains: 000659 and 000664, respectively) and housed in the BSL-3 at WVU. Infected mice were euthanized 8 weeks post-infection (15 weeks of age) with carcasses being placed in 10% formalin for 2 weeks followed by 70% ethanol; controls were euthanized at 12 weeks of age. Analysis of bone degradation in the left distal femur, left paw, and L4 vertebrae of the spine was performed using the Bruker SkyScan 1272 Micro-CT and the SkyScan 3D Software Suite at West Virginia University's Animal Models and Imaging Facility (Table 3). All graphs were made using Prism by GraphPad; all data was analyzed using an unpaired t-test.

Antibiotic and ELP-004 Mouse Model

Female 8-week C3H/HeJ (n = 27) mice were received (Jackson Lab, strain: 000659) and individually housed. Mice were weighed and distributed equally amongst the treatment groups by weight. The compounds used were prepared based on an estimated average weight of 20 g and a maximum gavage volume of 200 μL (Table 5). ELP-004 and Vehicle were prepared in nanoparticles by Werner Geldenhuys. Rifampicin (Calbiochem, 557303-1GM) and isoniazid

(Sigma, I3377-5G) were used at concentrations of 25 and 10 mg/kg and prepared at 10 and 4 mg/mL solutions for 50 µL, respectively. Stock solutions for RIF and INH were prepared in sterile saline (2X) at 20 and 8 mg/mL, respectively. The RIF- and INH-only treatments were diluted to 1X in sterile saline and the RIF + INH treatments were mixed 1:1. The mice were dosed for 7 days then euthanized by cervical dislocation 1.5 hours after the final dose. The weights of the mice, left kidneys, livers, and spleens were collected; the tissues collected were plasma, bone marrow from the right rear leg, the left kidney fixed in formalin for histology, and the liver (cut into 3 pieces: 2 pieces frozen for RNA and protein extraction and 1 piece for histology). All graphs were made using Prism by GraphPad; data was analyzed using an ordinary one-way ANOVA.

qPCR Analysis of the Liver

The liver was homogenized in 1 mL of a mastermix of TRIzol (Invitrogen, 15596036) and 20x Pierce Premium-Grade TCEP HCl (PG82020), and the RNA transferred to a separate Eppendorf tube. Chloroform (0.2 mL) was added to each tube, vortexed, and incubated for 3 minutes. The samples were then centrifuged for 15 minutes at 12,000 RCF at 4°C. The aqueous phase was transferred to another Eppendorf tube, and 1 µL of GlycoBlue (Invitrogen, AM9515) was added to each tube; the phenol-chloroform phase was discarded. Then, 0.5 mL of isopropanol was added to the aqueous phase and stored overnight at -20°C. Following overnight storage, the samples were centrifuged for 10 minutes at 12,000 RCF at 4°C. The pellet was resuspended in 1 mL of 75% ethanol, vortexed briefly, and then centrifuged for 5 minutes at 7600 RCF at 4°C. The supernatant was discarded and the pellets were left to air dry for 10 minutes. The pellets were resuspended in 44 µL of RNase-free water and frozen at -80°C. For analysis, the samples were thawed, and a DNase treatment was conducted using the DNA-*free* Kit (AM1906) by Ambion as

instructed in the kit. Concentrations of RNA were assessed using a Nanodrop. RNA used in the cDNA reaction was normalized to a volume of 500 ng per sample. The cDNA synthesis reaction was carried out using the iScript cDNA Synthesis Kit from Bio-Rad (1708890) for a volume of 40 µL. Amplification of the genes was carried out by using the Applied Biosystems GeneAmp PCR System 9700. The cDNA samples were frozen at -20℃ prior to qPCR analysis. The cDNA, primers, and SYBR Green Supermix (Bio-Rad, 1725274), were thawed over ice. cDNA (2 µL) was placed in triplicate into Bio-Rad Hard Shell qPCR plates followed by 18 µL of master mix (SYBR Green Supermix + primers). The microplate was sealed using Seal Type B and a flat white rubber card to ensure seal. The plate was vortexed briefly then centrifuged for 1 minute at 300 RCF. Plates were analyzed using the Bio-Rad CFX OPUS Real-Time PCR System. Statistical analysis was performed using Prism by GraphPad; the data was analyzed using an ordinary one-way ANOVA.

Western Blot Assessment of CYP Enzymes

Livers were homogenized in 400 µL of a lysis buffer containing 1X MPER (Thermo Scientific, 78501) and 1x Halt Protease Inhibitor Cocktail (ThermoFisher, 78420). Samples were then vortexed for 45 minutes, with a single freeze-thaw in liquid nitrogen occurring approximately 20 minutes after the vortexing began. The lysate was transferred to an Eppendorf tube, and the samples were spun for 15 minutes at 12,000 RCF at 4℃. The supernatant was placed in another tube, and the samples were spun again at the same settings to remove lipid layer. A BCA assay was performed using the Pierce BCA Protein Assay Kit (23225). The volume of protein needed was calculated based on using 0.5 µg/mL well on the gel. Samples and PageRuler Plus Prestained Protein Ladder (ThermoFisher, 26619) were loaded onto a Bolt 4-12% Bis-Tris Plus gel

(ThermoFisher, NW04120BOX) and run at 200V for 30 minutes. The gel was transferred to a PVDF membrane (Invitrogen, IB24002) using the iBlot2 on setting P_o. The membrane was blocked for 1 hour on a shaker at room temperature using Superblock T20 (ThermoFisher, 37516). The membrane was incubated with 10 mL of CYP1A2 antibody (Proteintech, 19936-1-AP, 1:1000) overnight. The blot was washed 3x for 10 minutes with TBST, then 10 mL of the HRP-conjugated Goat anti-Rabbit (Invitrogen, A16104, 1:10,000) was added to the blot and shaken for 45 minutes. The blot was washed 2x with TBST, 1x with TBS, and Supersignal West Pico PLUS Chemiluminescent Substrate (ThermoFisher, 21059) was used to detect the protein. The blot was visualized using the iBright Imaging System (Invitrogen, FL1500). The blot was stripped using Restore Western Blot Stripping Buffer (ThermoFisher, 21059) for 15 minutes, washed 3x in TBS, and blocked for 1 hour. β-Actin (10 mL; BD Pharmingen, 612656, 1:5000) was added to the blots for one hour, then the blots were washed 3x with TBST and the HRP Goat anti-Mouse (BD Pharmingen, 554002, 1:5000) was added for 45 minutes. The blot was washed 2x with TBST and 1x with TBS, then visualized again using Supersignal West Pico PLUS Chemiluminescent Substrate and the iBright Imaging System. Analysis was performed using the iBright Analysis Software. Statistical analysis was performed using Prism 9 by GraphPad; the data was analyzed using an ordinary one-way ANOVA.

Histological Analysis

Histological staining of the livers and kidneys was performed by the Department of Pathology, Anatomy, and Laboratory Medicine at West Virginia University. Livers and kidneys isolated from mice treated with rifampin, isoniazid, ELP-004, or a combination were H & E stained to observe the morphology of liver and kidney cells.

Results

Determining a Mouse Model for Tuberculosis Infection

There is no gold standard model for evaluating tuberculosis in a mouse model. Common models include BALB/c, C57BL/6, and C3HeB/FeJ with the main differentiating factor being susceptibility to infection (Singh and Umesh, 2018). C57BL/6 (B6) mice have decreased susceptibility to infection due to increased post-infection survival with a decline in CFUs with the onset of adaptive immunity (Singh and Umesh, 2018). C3HeB/FeJ (C3H) have increased susceptibility to infection with *Mtb* and can form necrotic lesions similar to those found in humans (Singh and Umesh, 2018). In order to determine the best model for observing OAT, C57BL/6 and C3H/HeJ mice were infected with *Mtb* for 8 weeks and bone degradation in the spines and left distal femur were assessed. Settings and definitions used to analyze the results are in Tables 3 and 4. Results show a significant decrease in trabecular number and BS/BV and an increase in trabecular separation in the distal femur of B6 mice; the spines show no significant differences between naive and infected spines in the B6 mice (Fig. 6a - b). The C3H mice have a statistically significant increase in trabecular thickness but a significant increase in trabecular separation and a decrease in number and BS/BV (Fig. 6c - d). These results are conflicting as an increase in trabecular thickness would not indicate a loss of bone. Data from the spines of C3H mice also indicate bone loss as there is a significant decrease in trabecular number and BS/BV. From this, we determined that a C3H model would be best for any continuing studies on the investigation of TB.

Determining Drug Interactions Between First-Line Antibiotics and ELP-004

To evaluate the metabolic interactions between ELP-004 and rifampin and isoniazid, 27 naive C3H mice, divided into six groups, were treated with vehicle, rifampin, isoniazid, ELP-004 or a combination for seven consecutive days (Table 5). The weights of the mice, kidneys, livers, and spleens were not significantly different among the 6 groups (Fig. 7a-d). Assessment of *Cyp1a2, Cyp2d22, Cyp2b10, Cyp3a16, Cyp3a11,* and *Cyp3a41a/b* was done using qPCR. Following results from qPCR, the protein expression of CYP1A2 and CYP2B10 was performed using a western blot.; CYP enzymes examined represent those found in mice but are comparable to those found in humans (Table 6). Results showed significant changes in expression of *Cyp1a2* and *Cyp2b10* (Fig. 7e). Upregulated expression in both groups resulted from ELP-004. It was previously established that ELP-004 induces *Cyp1a2* and *Cyp2b10* in mice (McCall et al., unpublished). To confirm the protein expression of *Cyp1a2* and *Cyb2b10* in the liver, a western blot was performed. Results showed no significant differences in protein expression in *Cyp1a2* (Fig. 7f). Protein expression of *Cyp2b10* was significantly increased in treatments including ELP-004 (Fig. 7g). These data suggest that although *Cyp1a2* mRNA is increased with ELP-004 treatment, the protein expression is not altered in the same manner. Further studies are needed, however, possible explanations include decreased CYP1A2 protein translation or increased protein degradation. Expression of *Cyp2b10* mRNA and CYP2B10 protein were increased following ELP-004 treatment. This suggests that CYP2B10, human equivalent CYP2B6, is one of the primary CYP enzymes induced by ELP-004 (Table 6).

Combination Treatment of ELP-004, Rifampin, and Isoniazid Does Not Lead to Overt Morphological Changes

Livers and kidneys isolated from mice treated with rifampin, isoniazid, ELP-004, or a combination were H & E stained to observe the morphology of liver and kidney cells. No overt morphological changes were observed in liver or kidney cells between all treatment groups (Fig. 10).

Discussion

Although difficulties with the in vitro model stalled progression of Aim 1, ELP-004 was able to knock down multi-syncytial formation in both RANKL and H37Rv *Mtb* wells. The current treatment for OAT is the standard of care used for all TB infections. While elimination of *Mtb* is important to eradicate the disease, antibiotic treatment alone does not resolve any bone degeneracies or nerve damage that result from a *Mtb* infection in the bones and joints. The goal of this Aim was to determine whether the novel compound, ELP-004, could be used in combination with antibiotic treatment to diminish bone loss in OAT patients. To determine an ideal mouse model for studying TB infection, well-established mouse models were compared for bone loss. Although there were some overlapping similarities regarding bone loss between B6 and C3H mice, the C3H mice showed a significant bone loss in both the distal femur and in the spine. Naïve C3H mice treated with combination therapy saw no significant changes in body weight or the weights of their livers, kidneys, or spleens. Additionally, there was increased mRNA expression in *Cyp1a2* and *Cyp2b10* and increased protein expression in CYP2B10. Similar results were observed in mice following 8 weeks of treatment with ELP-004 (McCall et al., unpublished). Increased mRNA

expression but no change in protein expression regarding CYP1A2 could mean a few different things. Potentially, the protein could be degraded quickly following translation or there may not be increased translation. Increased mRNA and protein expression for CYP2B10 strongly suggests that ELP-004 induces this enzyme in mice; this equates to CYP2B6 in humans (Table 6).

Histological staining revealed no overt differences between the treatment groups. This coincides with the weight data confirming that combination therapy likely does not lead to hepatotoxic effects, though further studies will be needed to assess the effects of long-term treatment.

Future work would further establish the impact the combination treatment has on the liver and the interactions between rifampin, isoniazid, and ELP-004. The liver could be fluorescently stained to observe what cells are responsible for the metabolism of the drugs. Additionally, an infected mouse model would need to be used to determine whether ELP-004 can be used in combination with all first-line antibiotics for the elimination of TB and bone erosion. These data show promise for using ELP-004 to treat bone erosion in tuberculosis patients. With no currently established treatments for OAT, this could prevent long-term difficulties and deformities prominent in those with osteoarticular tuberculosis.

Figures

		Knee and Paw		Spine	
Micro-CT Settings	Camera Binning	2x2 (2016 x 1344)		2x2 (2016 x 1344)	
	Pixel Size	7 μm		5 μm	
	Filter	Al .25 mm		Al .25 mm	
	Voltage	60 kV		60 kV	
	Source Current	166 μA		166 μA	
Reconstruction	Beam Hardening	20%		20%	
	Ring Artifact Reduction	8-12		8-12	
	Histogram	0 - 0.12		0 - 0.12	
CTAn	Offset	62	73	55	55
	Selection	249	249	459	429
	Threshold	255/85	255/107	255/95	255/94
		B6	C3H	B6	C3H

Table 3. Setting used to analyze the knee, paw, and spine of B6 and C3H mice using Bruker Micro-CT systems.

Trabecular Thickness (Tb. Th.)	mm; a measure of 3D thickness by virtual sphere-fitting
Trabecular Separation (Tb. Sp.)	mm; the diameter of the space measured as relating to Tb. Th.
Trabecular Number (Tb. N.)	1/mm; the spatial density of internal structures
Bone Surface/Bone Volume (BS/BV)	1/mm; provides a general indication of structural complexity
Bone Surface/Total Volume (BS/TV)	1/mm; the ratio of segmented bone surface to bone volume
Bone Volume/Total Volume (BV/TV)	%; a key parameter in indicating spatial density

Table 4. Definitions of measurements analyzed by Bruker SkyScan 3D Software.

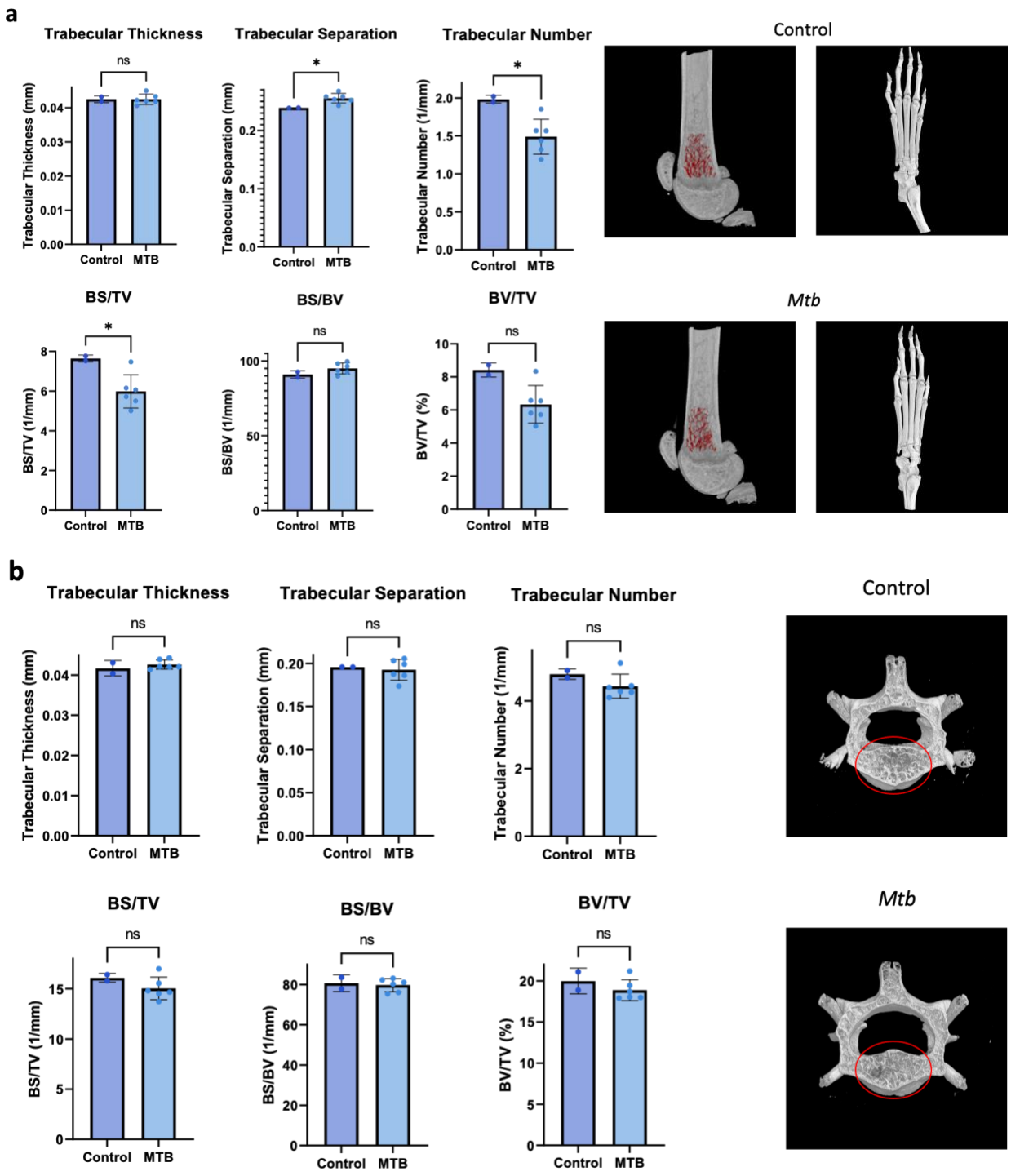

Figure 6. (a) Analysis of trabecular bone in the distal femur of B6 mice with representative images of the bone analyzed. Paws are measured using qualitative analysis. (b) Analysis of trabecular bone in the L4 vertebrae of the spine with representative images of the bone analyzed.

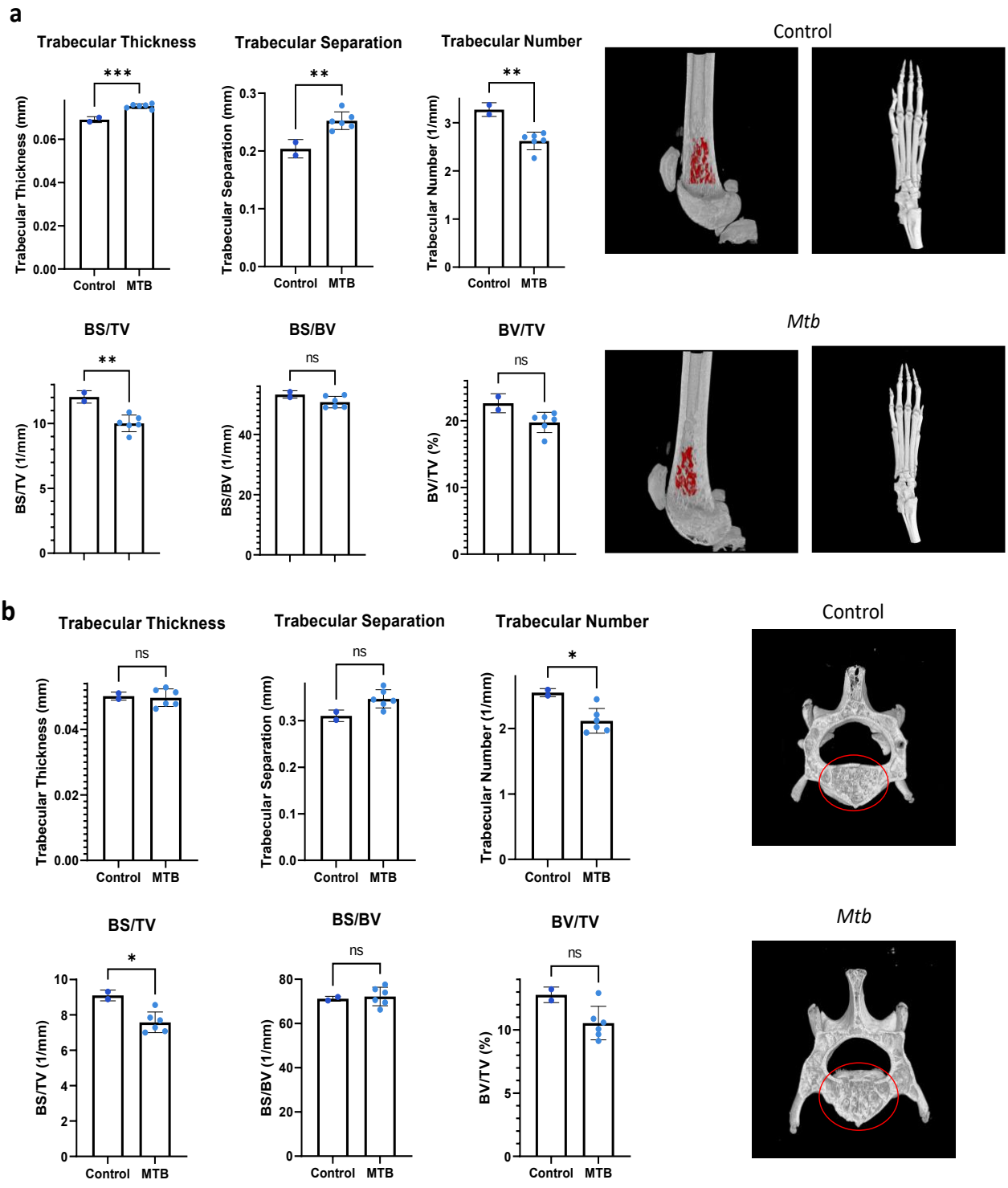
a
Trabecular Thickness
Trabecular Separation
Trabecular Number
Control
Trabecular Thickness (mm)
Trabecular Separation (mm)
Trabecular Number (1/mm)
***
**
**
Control MTB
BS/TV
BS/BV
BV/TV
Mtb
BS/TV (1/mm)
BS/BV (1/mm)
BV/TV (%)
**
ns
ns
b
Trabecular Thickness
Trabecular Separation
Trabecular Number
Control
ns
ns
*
BS/TV
BS/BV
BV/TV
Mtb
*
ns
ns

Figure 7. (a) Analysis of trabecular bone in the distal femur of C3H mice with representative images of the bone analyzed. Paws are measured using qualitative analysis. (b) Analysis of trabecular bone in the L4 vertebrae of the spine with representative images of the bone analyzed.

Treatment Group	Number of Mice	Vehicle (uL)	ELP-004 (uL)	RIF only (uL)	INH only (uL)	RIF + INH (uL)	Saline (uL)
Vehicle	3	150	-	-	-	-	50
RIF (25 mg/kg) + Vehicle	5	150	-	50	-	-	-
INH (10 mg/kg) + Vehicle	5	150	-	-	50	-	-
ELP-004 (4.5 mg/mouse)	5	-	150	-	-	-	50
RIF + INH + Vehicle	4	150	-	-	-	50	-
RIF + INH + ELP-004	5	-	150	-	-	50	-

Table 5. Treatment groups and drug distribution for the *Mtb* Antibiotic + ELP-004 mouse study.

Human Gene	Mouse Gene
CYP3A4	*Cyp3a11*
	Cyp3a16
	Cyp3a41a/B
CYP1A2	*Cyp1a2*
CYP2B6	*Cyp2b10*
CYP2D6	*Cyp2d22*

Table 6. Comparison of human and mouse CYP enzymes analyzed using qPCR

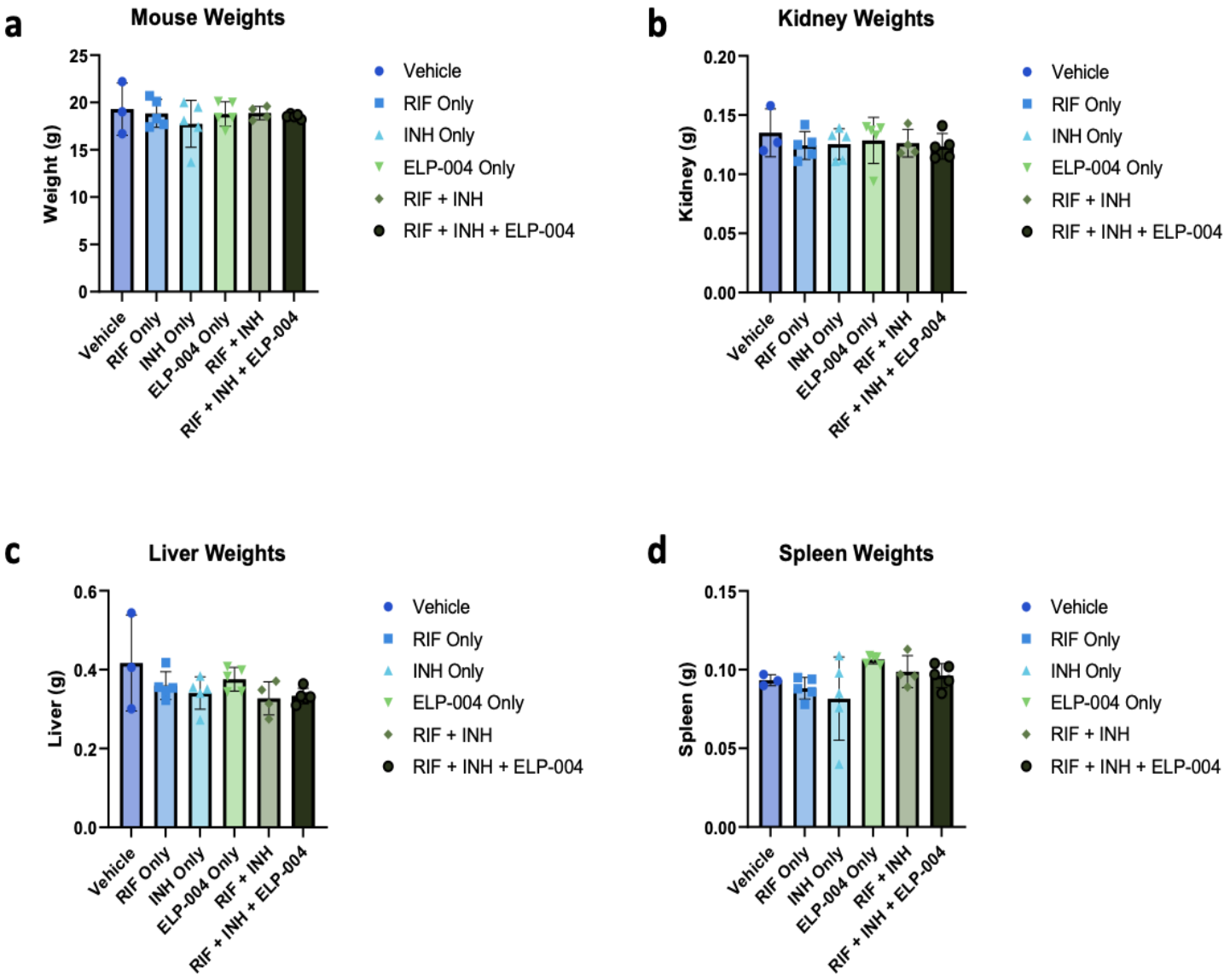

Figure 8. Weights of (a) mice, (b) kidney, (c) liver, and (d) spleens following 7 days of treatment with vehicle, rifampin (RIF), isoniazid (INH), ELP-004, or a combination.

a

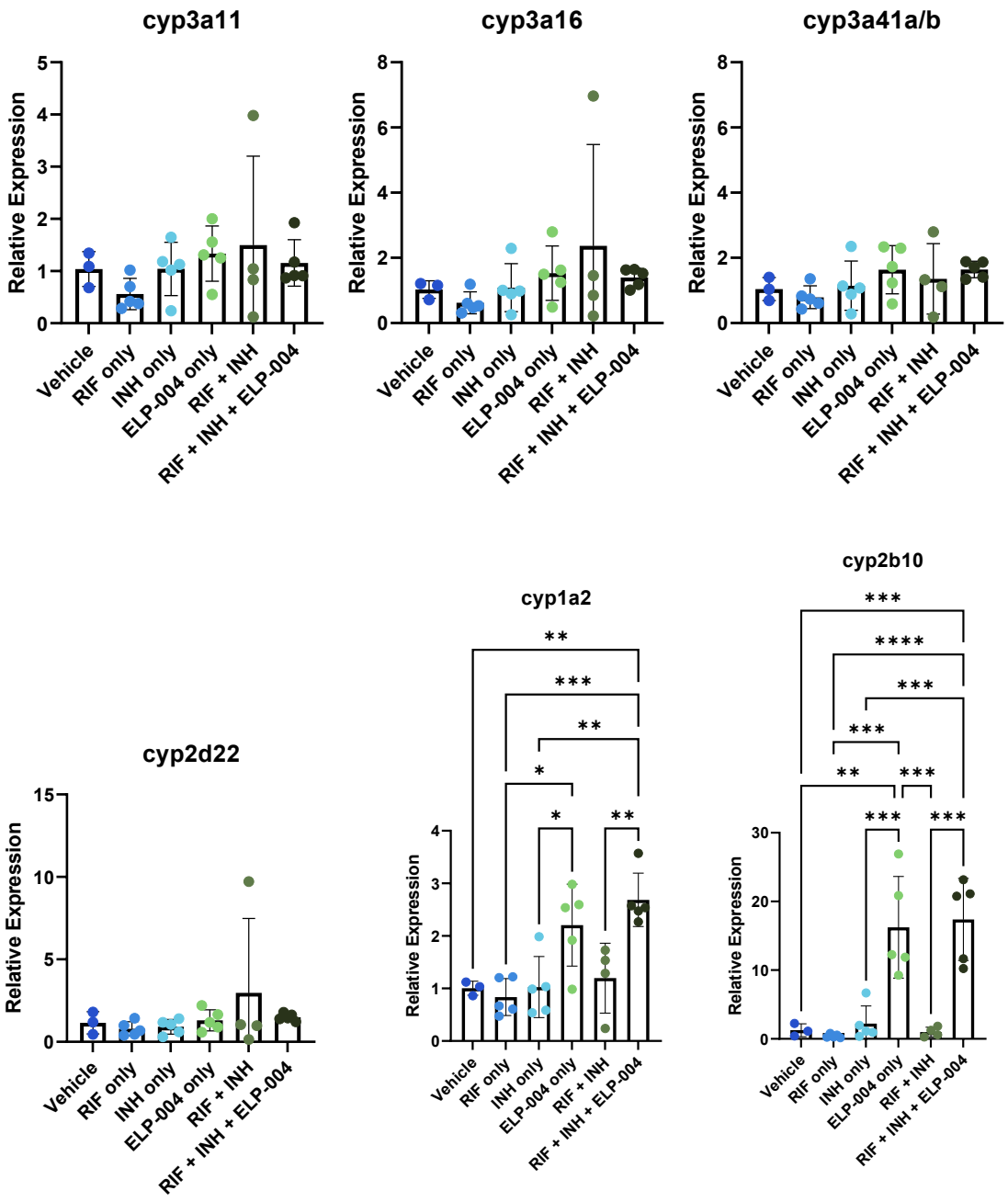
cyp3a11
cyp3a16
cyp3a41a/b
cyp2d22
cyp1a2
cyp2b10
Relative Expression
Vehicle
RIF only
INH only
ELP-004 only
RIF + INH
RIF + INH + ELP-004

b

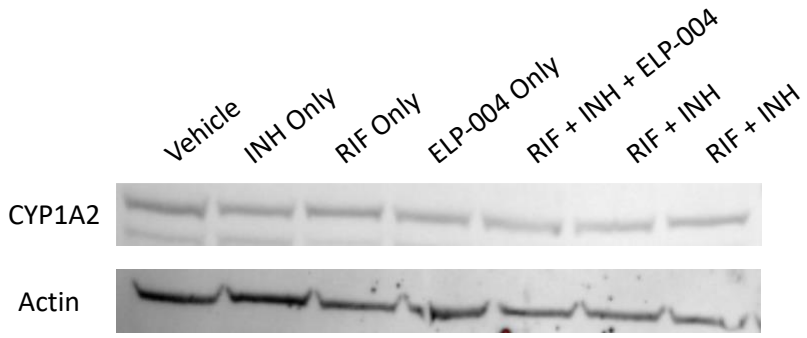

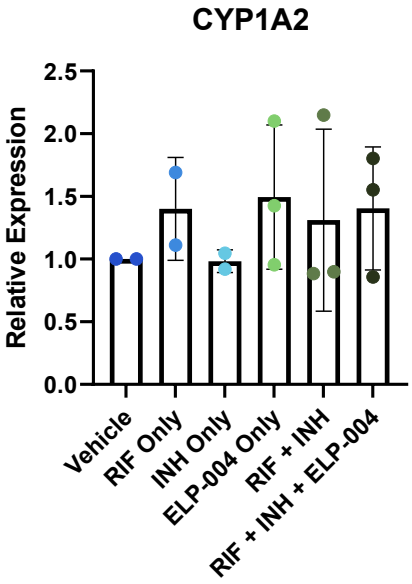

c

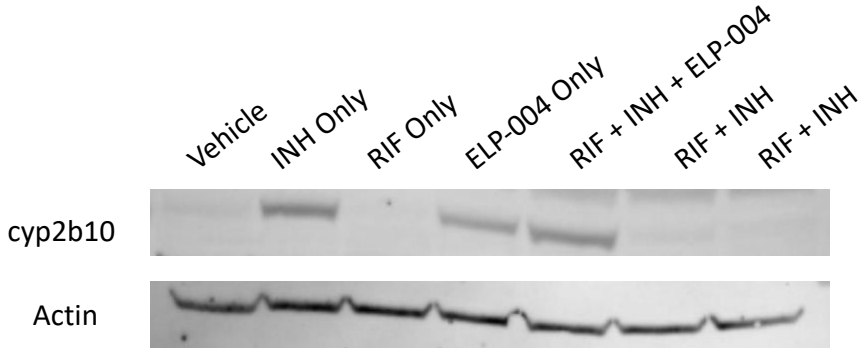

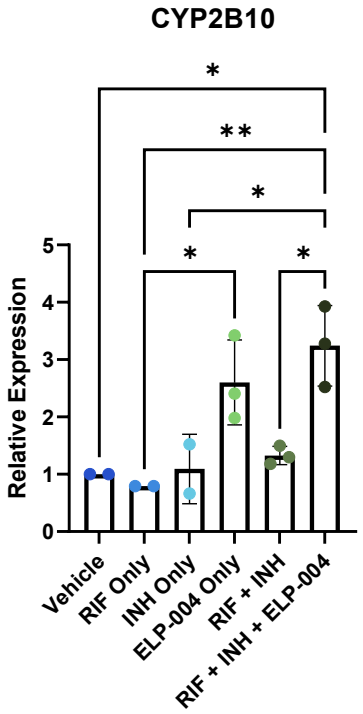

Figure 9. (a) qPCR analysis of *Cyp3a11*, *Cyp3a16*, *Cyp3a41a/b*, *Cyp2b22*, *Cyp1a2*, *Cyp2b10*.

(b) Representative image of western blot form CYP1A2 and analysis of western blots. (c) Representative image of western blot form CYP2B10 and analysis of western blots. Analysis of western blots combines data from two blots.

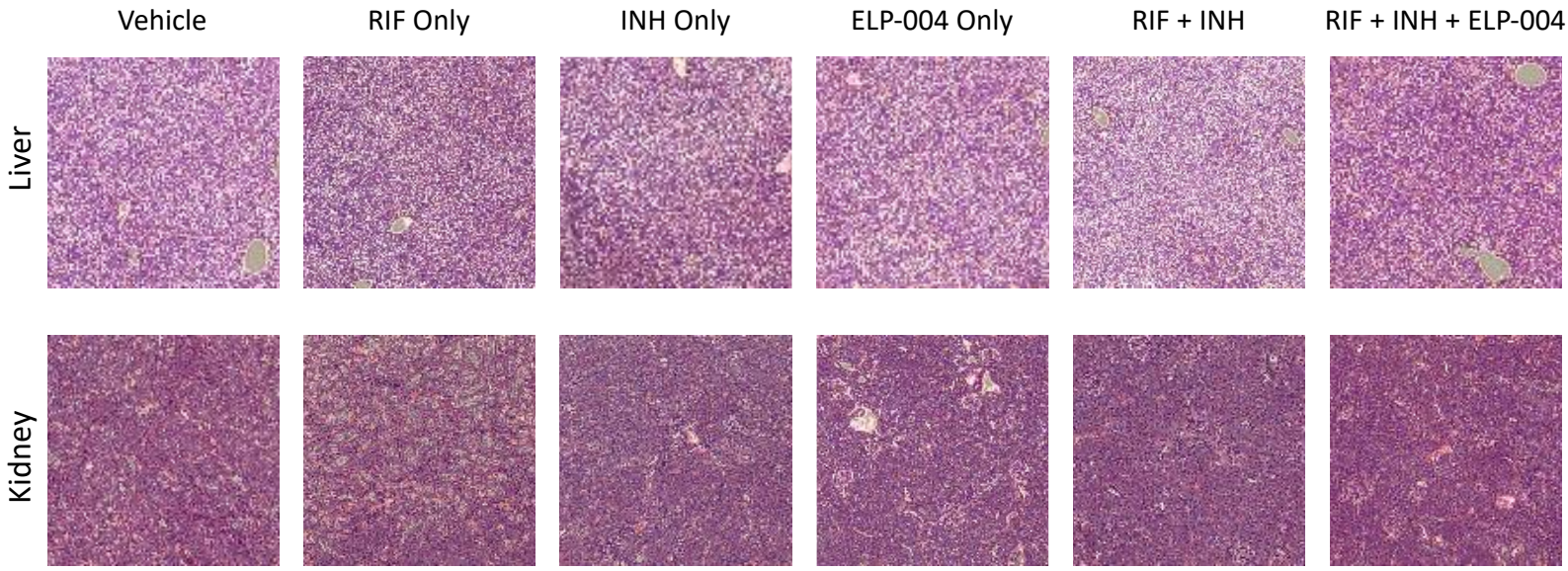

Figure 10. H & E staining of livers and kidneys isolated from C3H mice.

Bibliography

Al-Sayyad, Mohammed J, and Lutf A Abumunaser. Tuberculous Arthritis Revisited as a Forgotten Cause of Monoarticular Arthritis. *Annals of Saudi Medicine*, U.S. National Library of Medicine, 2011, https://www.ncbi.nlm.nih.gov/pmc/articles/PMC3156518/.

ATCC. "Raw 264.7 - Tib-71 | ATCC." *ATCC*, ATCC, https://www.atcc.org/products/tib-71.

Centers for Disease Control and Prevention. "Chapter 6 Treatment of Tuberculosis Disease - Centers for Disease ..." *Centers for Disease Control and Prevention*, Centers for Disease Control and Prevention, https://www.cdc.gov/tb/education/corecurr/pdf/chapter6.pdf.

Centers for Disease Control and Prevention. "Treatment for TB Disease." *Centers for Disease Control and Prevention*, Centers for Disease Control and Prevention, 7 Mar. 2022, https://www.cdc.gov/tb/topic/treatment/tbdisease.htm.

"Symptoms of Pulmonary and Extrapulmonary TB Disease." *Centers for Disease Control and Prevention*, Centers for Disease Control and Prevention, https://www.cdc.gov/tb/webcourses/Course/chapter4/4_diagnosis_of_tb_disease_4_clinical_practices_symptoms_of_pulmonary_and_extrapulmonary_tb_disease.html.

Delogu, Giovanni, et al. "The Biology of Mycobacterium Tuberculosis Infection." *Mediterranean Journal of Hematology and Infectious Diseases*, U.S. National Library of Medicine, 16 Nov. 2013, https://www.ncbi.nlm.nih.gov/pmc/articles/PMC3867229/.

Dorhoi, Anca, and Stefan H.E. Kaufmann. "Tumor Necrosis Factor Alpha in Mycobacterial Infection." *Seminars in Immunology*, Academic Press, 10 May 2014, https://www.sciencedirect.com/science/article/abs/pii/S1044532314000499.

Guillouzouic, Aurélie, et al. "Treatment of Bone and Joint Tuberculosis in France: A Multicentre Retrospective Study." *Journal of Clinical Medicine*, U.S. National Library of Medicine, 5 Aug. 2020, https://www.ncbi.nlm.nih.gov/pmc/articles/PMC7464673/.

Hussain, Zahir, et al. "Metabolism and Hepatotoxicity of Pyrazinamide, an Antituberculosis Drug." *Drug Metabolism and Disposition: the Biological Fate of Chemicals*, U.S. National Library of Medicine, Aug. 2021, https://www.ncbi.nlm.nih.gov/pmc/articles/PMC8407665/.

JW, Putney. "Capacitative Calcium Entry: From Concept to Molecule." *Immunological Reviews*, U.S. National Library of Medicine, 10 Sept. 2009, https://pubmed.ncbi.nlm.nih.gov/19754887/.

Kodama, Joe, and Takashi Kaito. "Osteoclast Multinucleation: Review of Current Literature." *MDPI*, Multidisciplinary Digital Publishing Institute, 8 Aug. 2020, https://www.mdpi.com/1422-0067/21/16/5685.

Kong, Lingbo, et al. "Overview of raw264.7 for Osteoclastogensis Study: Phenotype and Stimuli." *Journal of Cellular and Molecular Medicine*, U.S. National Library of Medicine, May 2019, https://www.ncbi.nlm.nih.gov/pmc/articles/PMC6484317/.

Lampiasi, Nadia, et al. “Osteoclasts Differentiation from Murine Raw 264.7 Cells Stimulated by RANKL: Timing and Behavior.” *Biology*, U.S. National Library of Medicine, 4 Feb. 2021, https://www.ncbi.nlm.nih.gov/pmc/articles/PMC7915339/.

Lee, Ji Yeon. "Diagnosis and Treatment of Extrapulmonary Tuberculosis." *Tuberculosis and Respiratory Diseases*, U.S. National Library of Medicine, Apr. 2015, https://www.ncbi.nlm.nih.gov/pmc/articles/PMC4388900/.

Liu, Wei, et al. "Mycobacterium Tuberculosis Infection Increases the Number of Osteoclasts and Inhibits Osteoclast Apoptosis by Regulating TNF-α-Mediated Osteoclast Autophagy." *Experimental and Therapeutic Medicine*, U.S. National Library of Medicine, Sept. 2020, https://www.ncbi.nlm.nih.gov/pmc/articles/PMC7401307/.

Lynch, Tom, and Amy Price. “"The Effect of Cytochrome P450 Metabolism on Drug Response, Interactions, and Adverse Effects." *American Family Physician*, 1 Aug. 2007, https://www.aafp.org/pubs/afp/issues/2007/0801/p391.html.

McDonnell, Anne M, and Cathyyen H Dang. "Basic Review of the Cytochrome P450 System." *Journal of the Advanced Practitioner in Oncology*, U.S. National Library of Medicine, July 2013, https://www.ncbi.nlm.nih.gov/pmc/articles/PMC4093435/.

MedlinePlus. “ACP5 Gene: Medlineplus Genetics.” *MedlinePlus*, U.S. National Library of Medicine, 1 Dec. 2013, https://medlineplus.gov/genetics/gene/acp5/.

N, Arathi, et al. “OSTEOARTICULAR Tuberculosis-A Three Years' Retrospective Study.” *Journal of Clinical and Diagnostic Research : JCDR*, U.S. National Library of Medicine, Oct. 2013, https://www.ncbi.nlm.nih.gov/pmc/articles/PMC3843457/.

Natarajan, Arvind, et al. "A Systemic Review on Tuberculosis." *Indian Journal of Tuberculosis*, Elsevier, 28 Feb. 2020, https://www.sciencedirect.com/science/article/abs/pii/S0019570720300305?via%3Dihub.

O'Connor, Courtney, and Mark F. Brady. "Isoniazid - StatPearls - NCBI Bookshelf." *National Library of Medicine* , National Library of Medicine, 8 Apr. 2022, https://www.ncbi.nlm.nih.gov/books/NBK557617/.

Padda, Inderbir S., and Kona Muralidhara Reddy. "Antitubercular Medications - Statpearls - NCBI Bookshelf." *National Library of Medicine,* National Library of Medicine, 30 Nov. 2022, https://www.ncbi.nlm.nih.gov/books/NBK557666/.

Pigrau-Serrallach, Carlos, and Dolores Rodríguez-Pardo. "Bone and Joint Tuberculosis." *European Spine Journal: Official Publication of the European Spine Society, the European Spinal Deformity Society, and the European Section of the Cervical Spine Research*

Society, U.S. National Library of Medicine, June 2013, https://www.ncbi.nlm.nih.gov/pmc/articles/PMC3691411/.

Rabahi, Marcelo Fouad, et al. “Tuberculosis Treatment.” *Jornal Brasileiro De Pneumologia : Publicacao Oficial Da Sociedade Brasileira De Pneumologia e Tisilogia*, U.S. National Library of Medicine, 2017, https://www.ncbi.nlm.nih.gov/pmc/articles/PMC5792048/.

Rao, Hongwei, et al. "Corning® Osteo Assay Surface: A New Tool to Study Osteoclast and Osteoblast Differentiation and Function." *Corning*, Corning Incorporated, https://www.corning.com/catalog/cls/documents/application-notes/snappshots_CLS_AN_144_osteo_assay.pdf.

Seung, Kwonjune J, et al. "Multidrug-Resistant Tuberculosis and Extensively Drug-Resistant Tuberculosis." *Cold Spring Harbor Perspectives in Medicine*, U.S. National Library of Medicine, 27 Apr. 2015, https://www.ncbi.nlm.nih.gov/pmc/articles/PMC4561400/.

Singh, Amit Kumar, and Umesh D Gupta. "Animal Models of Tuberculosis: Lesson Learnt." *The Indian Journal of Medical Research*, U.S. National Library of Medicine, May 2018, https://www.ncbi.nlm.nih.gov/pmc/articles/PMC6094516/.

Soysa, NS, and N Alles. "NF-Kappa b Functions in Osteoclasts." *Biochemical and Biophysical Research Communications*, U.S. National Library of Medicine, 2 Jan. 2009, https://pubmed.ncbi.nlm.nih.gov/18992710/.

Sundell, Jesper, et al. "Population Pharmacokinetics and Pharmacogenetics of Ethambutol in Adult Patients Coinfected with Tuberculosis and HIV." *Antimicrobial Agents and Chemotherapy*, U.S. National Library of Medicine, 27 Jan. 2020, https://www.ncbi.nlm.nih.gov/pmc/articles/PMC6985744/.

Suresh, Ashithkumar Beloor, et al. "Rifampin - StatPearls - NCBI Bookshelf." *National Library of Medicine*, National Library of Medicine, 13 Apr. 2022, https://www.ncbi.nlm.nih.gov/books/NBK557488/.

Taciak, Bartłomiej, et al. "Evaluation of Phenotypic and Functional Stability of Raw 264.7 Cell Line through Serial Passages." *PloS One*, U.S. National Library of Medicine, 11 June 2018, https://www.ncbi.nlm.nih.gov/pmc/articles/PMC5995401/.

"Tuberculosis (TB)." *World Health Organization*, World Health Organization, https://www.who.int/news-room/fact-sheets/detail/tuberculosis.

Tuli, S M. "General Principles of Osteoarticular Tuberculosis: Clinical Orthopaedics and Related Research®." *Clinical Orthopedics and Related Research*, Lippincott Williams and Wilkins, May 2002, https://journals.lww.com/clinorthop/fulltext/2002/05000/general_principles_of_osteoarticular_tuberculosis.3.aspx.

Xiao, Lan, and Yin Xiao. "The Autophagy in Osteoimmonology: Self-Eating, Maintenance, and Beyond." *Frontiers*, Frontiers, 8 July 2019, https://www.frontiersin.org/articles/10.3389/fendo.2019.00490/full.

Xu, Feng, and Steven L. Teitelbaum. "Osteoclasts: New Insights." *Nature News*, Nature Publishing Group, 29 Mar. 2013, https://www.nature.com/articles/boneres20133.

Zhao, Qingxiao, et al. "NFATC1: Functions in Osteoclasts." *The International Journal of Biochemistry & Cell Biology*, Pergamon, 24 Dec. 2009, https://www.sciencedirect.com/science/article/pii/S1357272509003719.

Zhou Shu-Feng, Drugs Behave as Substrates, Inhibitors and Inducers of Human Cytochrome P450 3A4, Current Drug Metabolism 2008; 9(4). https://dx.doi.org/10.2174/138920008784220664